

Relativistic positron scattering from heavy ground-state nuclei

D. H. Jakubassa-Amundsen

Mathematics Institute, University of Munich, Theresienstrasse 39,
80333 Munich, Germany

(Dated:)

Cross sections and spin asymmetries for elastic positron scattering and for the emission of positron bremsstrahlung in collision with nuclei of zero and half-integer spin are calculated within the relativistic partial-wave theory. For elastic scattering, comparison is made with the respective results from electron scattering by ^{208}Pb , ^{89}Y and ^{23}Na nuclei at high energies (up to 400 MeV). It is found that the difference between electron and positron intensities diminishes with energy, although the diffraction oscillations, which differ in phase for the two species, prevail up to the highest energies considered. Magnetic scattering strongly reduces the spin asymmetries for nuclei with spin, both for positrons and electrons. For the elementary process of bremsstrahlung the cross section, which is studied for the ^{197}Au and ^{208}Pb targets at low energies (1 – 30 MeV), increases with photon frequency for large scattering angles and small photon emission angles, in contrast to the usual behaviour of the doubly differential cross section, or of the triply differential cross section at small scattering angles.

1. INTRODUCTION

While spin asymmetries in low-energy elastic positron scattering from atoms have been investigated recently [1–4], high-energy scattering experiments from nuclei have concentrated on the measurement of differential cross sections. Such experiments on positron scattering from protons were aimed at investigating the two-photon exchange contribution [5, 6]. There exist also scattering experiments using heavier targets, including lead and bismuth, for which the corresponding theoretical calculations were carried out by means of the relativistic phase shift analysis [7–15]. In these investigations, emphasis was laid on the relative cross section difference between positron and electron impact as a function of scattering angle or momentum transfer, by using collision energies up to 450 MeV. With this method, information on the nuclear ground-state charge density could be obtained. In contrast, studies of the spin asymmetries in collisions beyond 1 MeV positron energy are scarce (see, e.g. [16, 17]).

For elastic electron scattering, on the other hand, the resulting polarization correlations are well known, as discussed thoroughly in the literature [18–20]. More recent theoretical work can be found in [21–23], but up to now systematic experiments on the spin asymmetry relating to electrons spin-polarized perpendicular to the scattering plane, the so-called Sherman function, exist only up to 14 MeV collision energy [24]. Actually, a few isolated measurements can be found at much higher energies, up to 3 GeV, in the context of two-photon effects and parity violation (see, e.g. [25, 26]).

Apart from being elastically scattered, the positron or electron will also emit bremsstrahlung in the field of the nucleus. In fact, a close relation between an elastically scattered electron and a circularly polarized bremsstrahlung photon with maximum possible energy was established for sufficiently high collision energy [27, 28]. The equivalence of these two processes at energies where the electron’s rest mass is of minor importance manifests itself in a similarity of the respective polarization correlations which describe the spin transfer of a beam particle to an outgoing particle in a helicity eigenstate (provided that in the bremsstrahlung process the scattered lepton is not observed).

Investigations concerning positron bremsstrahlung are scarce, based on the expectation that for fast particles there should not be much difference between electron and positron impact. Within the relativistic Dirac partial-wave (DW) theory, high-energy positron bremsstrahlung was in early work investigated analytically and numerically near the short-wavelength limit (SWL) [29, 30]. There is later work on the (angle-integrated) spectral distribution of positron bremsstrahlung, using the DW theory, but only for low collision energies up to 0.5 MeV [31]. A full theoretical account of the photon energy and angular distribution, including the linear polarization correlations between beam positron and photon (for unobserved scattered positrons), was given only recently in the regime 0.1 – 1 MeV [32].

For electron scattering, again much more work has been done. An investigation of the linear and circular bremsstrahlung polarization correlations, both experimentally and theoretically, is provided in [33–37], the theory being described in [38] and the polarization correlations being introduced in [33]. Recently, particularly for advancing to higher collision energies in the MeV region, the numerical DW code was optimized by introducing the complex-plane rotation method [39] for performing the radial integrals [40–42].

The present work concentrates on high-energy elastic scattering as well as on bremsstrahlung emission by positron impact in the MeV region, in comparison with the respective results for electron scattering. An overview over the theories is provided, which are subsequently used in the numerical calculations. In Section II elastic scattering from the spin-zero nucleus ^{208}Pb is considered, for which experimental cross section data on electron and positron scattering are available [8]. The influence of magnetic scattering is studied with the help of the distorted-wave Born approximation (DWBA) by choosing as targets the spin- $\frac{1}{2}$ nucleus ^{89}Y and the spin- $\frac{3}{2}$ nucleus ^{23}Na . For both nuclei, electron scattering data at 180° are available which isolate the magnetic contribution [43, 44]. Section III deals with positron bremsstrahlung in collision with ^{197}Au and ^{208}Pb nuclei. For the bremsstrahlung polarization correlations a sum rule, known from electron scattering investigations [45, 46], is probed for the positrons. The equivalence between elastically scattered positrons and bremsstrahlung in the vicinity of the SWL is explored in Section IV. The conclusion is drawn in Section V. Atomic units ($\hbar = m = e = 1$) are used unless otherwise indicated.

2. ELASTIC POSITRON SCATTERING

In order to derive the scattering states of a positron one has to apply charge conjugation. Given an electronic state of a bare nucleus, $\psi_{e^-}(\mathbf{r}, \boldsymbol{\zeta}, Z)$, with spin polarization $\boldsymbol{\zeta}$ and nuclear charge number Z , the respective state for a positron is obtained by means of [47, 48]

$$\psi_{e^+}(\mathbf{r}, \boldsymbol{\zeta}, Z) = i \gamma_2 \psi_{e^-}^*(\mathbf{r}, \boldsymbol{\zeta}, -Z) \quad (2.1)$$

with the Dirac matrix $\gamma_2 = \begin{pmatrix} 0 & \sigma_2 \\ -\sigma_2 & 0 \end{pmatrix}$, where $\sigma_2 = \begin{pmatrix} 0 & -i \\ i & 0 \end{pmatrix}$.

Thus, let us consider an incoming electron which impinges along the z -direction, being described within the relativistic partial-wave expansion [48, 49],

$$\psi_{i,e^-}^{(+)}(\mathbf{r}, \boldsymbol{\zeta}_i, Z) = \sum_{m_i=\pm\frac{1}{2}} a_{m_i} \sum_{\kappa_i} \sqrt{\frac{2l_i+1}{4\pi}} (l_i 0 \frac{1}{2} m_i | j_i m_i) i^{l_i} e^{i\delta_{\kappa_i}} \begin{pmatrix} g_{\kappa_i}(r) Y_{j_i l_i m_i}(\hat{\mathbf{r}}) \\ i f_{\kappa_i}(r) Y_{j_i l_i m_i}(\hat{\mathbf{r}}) \end{pmatrix}. \quad (2.2)$$

Then the respective positron function will be an outgoing state which reads

$$\psi_{i,e^+}^{(-)}(\mathbf{r}, \boldsymbol{\zeta}_i, Z) = i \sum_{m_i=\pm\frac{1}{2}} a_{-m_i}^* \sum_{\kappa_i} \sqrt{\frac{2l_i+1}{4\pi}} (-1)^{\frac{1}{2}-m_i} (l_i 0 \frac{1}{2} m_i | j_i m_i) (-i)^{l_i} e^{-i\delta_{\kappa_i}} \begin{pmatrix} f_{\kappa_i}(r) Y_{j_i l_i m_i}(\hat{\mathbf{r}}) \\ i g_{\kappa_i}(r) Y_{j_i l_i m_i}(\hat{\mathbf{r}}) \end{pmatrix}, \quad (2.3)$$

where g_{κ_i} and f_{κ_i} are, respectively, the large and small components of the radial Dirac function. Note that g_{κ_i} and f_{κ_i} interchange their role when switching from electron to positron. The positron phase shifts δ_{κ_i} as well as g_{κ_i} and f_{κ_i} in (2.3) result from solutions to the Dirac equation with negative potential, $-V(r)$. Furthermore, a_{m_i} are the coefficients of the spinors $\chi_{\frac{1}{2}} = \begin{pmatrix} 1 \\ 0 \end{pmatrix}$ and $\chi_{-\frac{1}{2}} = \begin{pmatrix} 0 \\ 1 \end{pmatrix}$, describing the direction of the polarization vector $\boldsymbol{\zeta}_i$, see (2.7) below. The symbol $(\cdot \cdot | \cdot)$ is a Clebsch-Gordan coefficient, and $Y_{j_l m}$ denotes a spherical harmonic spinor [50]. The quantum numbers $\kappa_i = \pm 1, \pm 2, \dots$ are interrelated with the angular momentum quantum numbers j_i and l_i by means of $\kappa_i = l_i$ and $l_i' = l_i - 1$ for $j_i = l_i - \frac{1}{2}$ as well as $\kappa_i = -l_i - 1$ and $l_i' = l_i + 1$ for $j_i = l_i + \frac{1}{2}$.

In a similar way, the positron function which corresponds to an outgoing final electron with momentum \mathbf{k}_f can be found to be

$$\psi_{f,e^+}^{(+)}(\mathbf{r}, \boldsymbol{\zeta}_f, Z) = i \sum_{\kappa_f m_f} \sum_{m_l m_s} Y_{l_f m_l}^*(\hat{\mathbf{k}}_f) b_{-m_s}^* (-1)^{\frac{1}{2}-m_s} (l_f m_l \frac{1}{2} m_s | j_f m_f) (-i)^{l_f} e^{i\delta_{\kappa_f}} \begin{pmatrix} f_{\kappa_f}(r) Y_{j_f l_f m_f}(\hat{\mathbf{r}}) \\ i g_{\kappa_f}(r) Y_{j_f l_f m_f}(\hat{\mathbf{r}}) \end{pmatrix}, \quad (2.4)$$

where Y_{lm} is a spherical harmonic function, and the coefficients b_{m_s} relate to the final polarization vector $\boldsymbol{\zeta}_f$.

A. Positron scattering from spin-zero nuclei

For near-spherical spin-zero nuclei the elastic scattering process can be expressed in terms of potential scattering. This implies that the nucleus is characterized solely by the nuclear potential which is obtained from the ground-state charge distribution, and that recoil is neglected. In fact, recoil effects during elastic scattering from spin-zero nuclei were investigated in [51] and were found to be small for collision energies up to several hundred MeV.

Within the phase shift analysis, the scattering amplitude for a particle of momentum \mathbf{k}_i and spin polarization ζ_i , being deflected by an angle θ , is given by

$$f_e(\zeta_i, \zeta_f, k_i, \theta) = \langle \chi_f | A + B \mathbf{n} \boldsymbol{\sigma} | \chi_i \rangle, \quad (2.5)$$

where ζ_f and $\mathbf{k}_f = k_f(\sin \theta, 0, \cos \theta)$ (setting $k_f = k_i$ in the recoil-free case) are, respectively, spin polarization and momentum of the scattered particle. Moreover, A and B are, respectively, the spin-conserving and spin-flip parts of the transition amplitude, $\mathbf{n} = \mathbf{e}_y$ is the normal to the scattering plane (spanned by \mathbf{k}_i and \mathbf{k}_f), $\boldsymbol{\sigma}$ is the vector of Pauli matrices, and χ_i, χ_f denote the spin states [48],

$$\chi_i = a_{\frac{1}{2}} \chi_{\frac{1}{2}} + a_{-\frac{1}{2}} \chi_{-\frac{1}{2}}, \quad \chi_f = b_{\frac{1}{2}} \chi_{\frac{1}{2}} + b_{-\frac{1}{2}} \chi_{-\frac{1}{2}}, \quad (2.6)$$

where for an arbitrary unit vector ζ_i , defined by the spherical angles α_s and φ_s with respect to the scattering plane, the coefficients are

$$a_{\frac{1}{2}} = \cos \frac{\alpha_s}{2} e^{-i\varphi_s/2}, \quad a_{-\frac{1}{2}} = \sin \frac{\alpha_s}{2} e^{i\varphi_s/2}. \quad (2.7)$$

The coefficients $b_{\pm\frac{1}{2}}$ for the final spin state are defined in the same way. If the scattered particle is in a helicity (+) state, which henceforth will be assumed, such that $\zeta_f = \hat{\mathbf{k}}_f$, one has $b_{\frac{1}{2}}^* = \cos \frac{\theta}{2}$ and $b_{-\frac{1}{2}}^* = \sin \frac{\theta}{2}$.

With (2.6), the scattering amplitude reduces to

$$f_e(\zeta_i, \zeta_f, k_i, \theta) = A (b_{\frac{1}{2}}^* a_{\frac{1}{2}} + b_{-\frac{1}{2}}^* a_{-\frac{1}{2}}) + iB (b_{-\frac{1}{2}}^* a_{\frac{1}{2}} - b_{\frac{1}{2}}^* a_{-\frac{1}{2}}). \quad (2.8)$$

The differential cross section for elastic scattering of unpolarized particles, which implies an average over χ_i as well as a sum over χ_f , is calculated from

$$\left(\frac{d\sigma}{d\Omega} \right)_0 = \frac{1}{2} \sum_{\zeta_i, \zeta_f} |f_e(\zeta_i, \zeta_f, k_i, \theta)|^2 = |A|^2 + |B|^2. \quad (2.9)$$

Since A and B , and hence the cross section, depend on the positron wavefunction only in terms of the phase shifts, the change from electron scattering to positron scattering is accomplished by replacing the nuclear charge number Z by $-Z$ in the nuclear potential when solving the Dirac equation for the phase shifts. This procedure also induces a sign change in f_e .

If, instead, the polarization of the particle is kept fixed, the cross section can be expressed in terms of the three spin asymmetries L, S , and R [18], pertaining to the three linear independent choices of ζ_i along the coordinate axes $\mathbf{e}_z = \hat{\mathbf{k}}_i$, $\mathbf{e}_y = \mathbf{k}_i \times \mathbf{k}_f / |\mathbf{k}_i \times \mathbf{k}_f|$ and $\mathbf{e}_x = \mathbf{e}_y \times \hat{\mathbf{k}}_i$ [18, 28],

$$\frac{d\sigma}{d\Omega}(\zeta_i, \zeta_f) = |f_e(\zeta_i, \zeta_f, k_i, \theta)|^2 = \frac{1}{2} \left(\frac{d\sigma}{d\Omega} \right)_0 [1 + S(\zeta_i \mathbf{e}_y) + L(\zeta_i \mathbf{e}_z) \zeta_{\pm} - R(\zeta_i \mathbf{e}_x) \zeta_{\pm}], \quad (2.10)$$

where $\zeta_{\pm} = \pm 1$ for outgoing particles in a helicity (\pm) state. Accordingly, the polarization correlations can be obtained in terms of relative cross section differences when the spin is flipped,

$$P(\zeta_i) = \frac{d\sigma/d\Omega(\zeta_i, \zeta_f) - d\sigma/d\Omega(-\zeta_i, \zeta_f)}{d\sigma/d\Omega(\zeta_i, \zeta_f) + d\sigma/d\Omega(-\zeta_i, \zeta_f)}, \quad (2.11)$$

and one defines $L = P(\mathbf{e}_z)$, $S = P(\mathbf{e}_y)$ and $R = P(-\mathbf{e}_x)$. The Sherman function S [52], requiring particles which are spin-polarized perpendicular to the scattering plane, is the easiest one to access experimentally since it is independent of the spin polarization ζ_f of the scattered particle [18].

B. Results for the elastic scattering from lead and from lighter spin-zero nuclei

For the ^{208}Pb nucleus, the charge density is available in terms of a Fourier-Bessel expansion [53] which provides an analytical representation of the nuclear potential [22]. The resulting Dirac equation is solved for the phase shifts with the help of the Fortran code RADIAL by Salvat et al [54]. When performing the sum over the phase shifts in the calculation of A and B (see, e.g. [22, 49]), a three-fold convergence acceleration as introduced by Yennie et al [55] is applied.

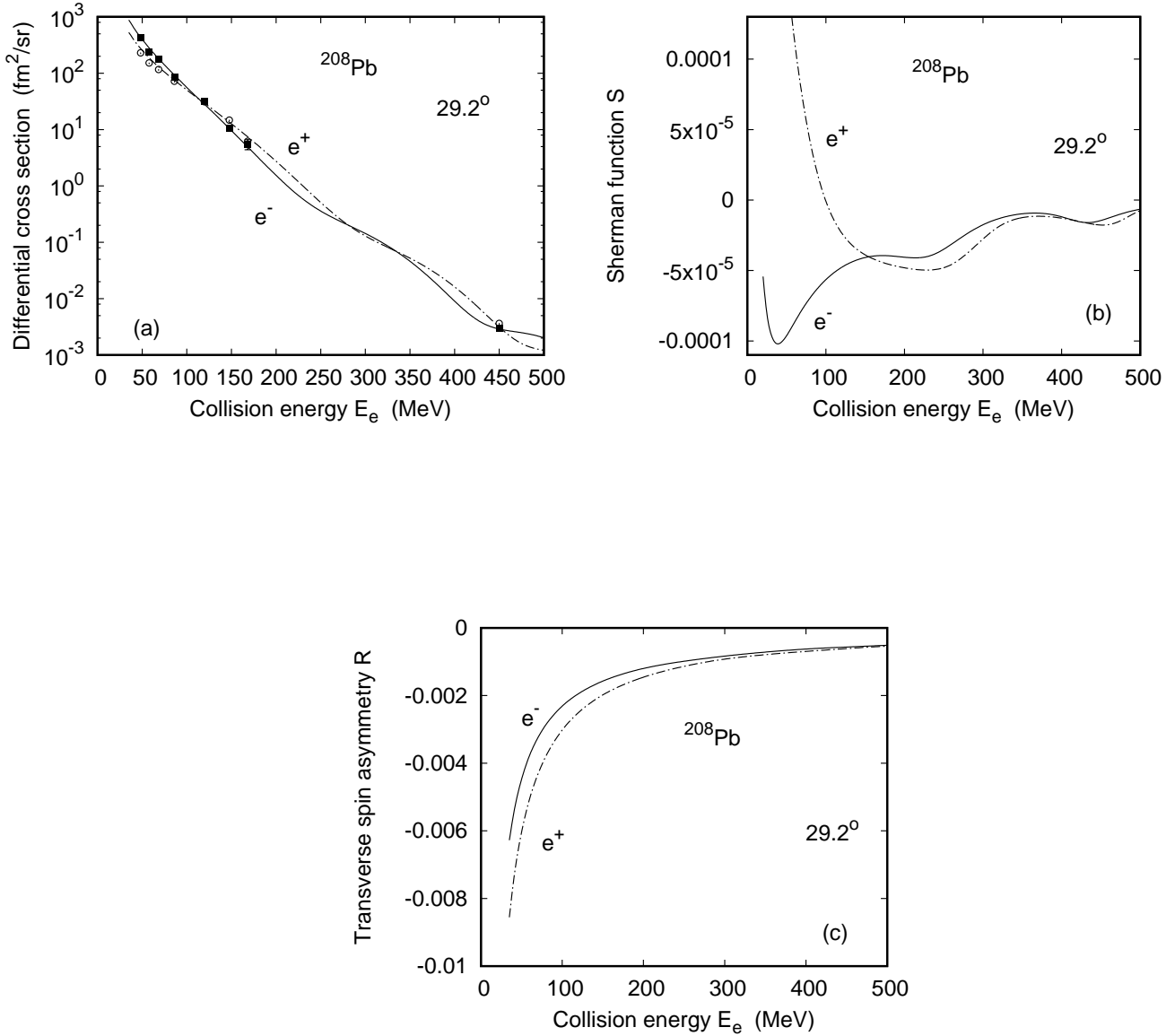


FIG. 1: Differential cross section $\frac{d\sigma}{d\Omega}$ (a) and spin asymmetries S (b) and R (c) for electrons and positrons scattered elastically from ^{208}Pb ($Z = 82$) as a function of collision energy E_e . The scattering angle is $\theta = 29.2^\circ$. —, electron impact; - - - -, positron impact. The experimental data in (a) below 200 MeV are from Miller and Robinson [8], those at 450 MeV are from Breton et al [14]: ■, electron scattering; ○, positron scattering.

Fig.1a shows the dependence of the differential cross section for a lead target on the collision energy at a fixed forward scattering angle $\vartheta_f = 29.2^\circ$. The electron and positron scattering data of [8, 14] are well reproduced by theory. The diffraction structures, which originate from interference effects induced by scattering off the individual protons when the collision energy is sufficiently high such that the projectile can penetrate the nuclear surface, are clearly visible at an energy above 50 MeV. There is a phase shift between the corresponding oscillations for positrons relative to those for electrons. This phase shift is interpreted in terms of an increase of the momentum k_i for electrons near the nucleus, due to the mutual attraction, and a reduced momentum for positrons due to the repulsive potential [11]. The nearly periodic diffraction pattern resembles the square of a spherical Bessel function $j_1(qR_N)$, with $q = |\mathbf{k}_i - \mathbf{k}_f| = 2k_i \sin \theta/2$ the momentum transfer to the nucleus and R_N the nuclear radius, which is an exact solution if the nucleus is approximated by a homogeneously charged sphere [19]. This periodicity disappears, however,

if the diffuseness of the nuclear surface is increased by at least a factor of 3.

In Figs.1b and 1c the spin asymmetries S and R are displayed. Since they are due to purely relativistic effects, they are very small for this forward angle. While $|R|$ decreases monotonously to zero with collision energy E_e , both for electrons and positrons, S shows the diffraction structures when $E_e \gtrsim 150$ MeV. The longitudinal polarization correlation L is always close to unity, according to the sum rule (4.2) for potential scattering [18].

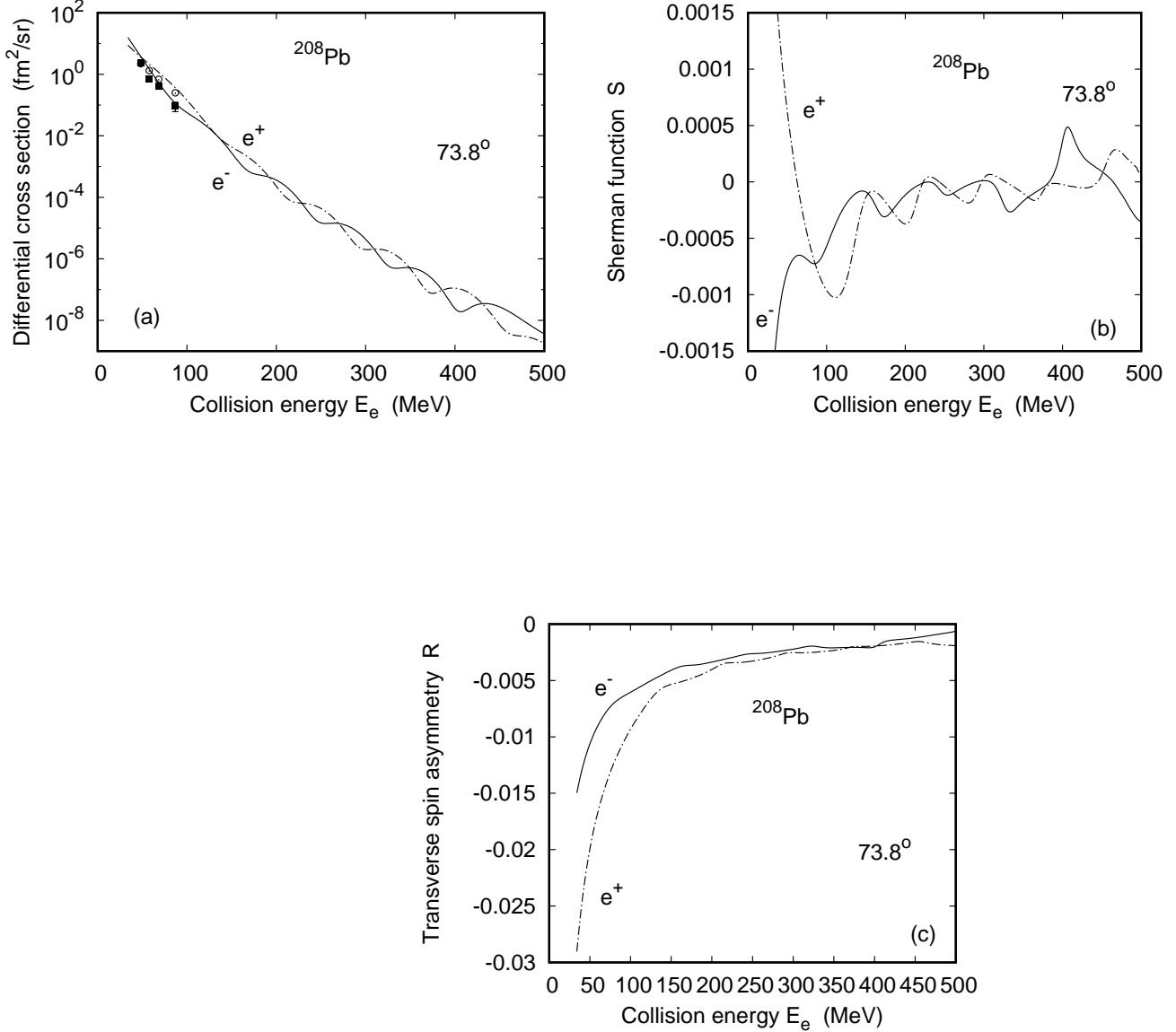


FIG. 2: Same as Fig.1, but for a scattering angle of 73.8° .

Fig.2 shows the respective quantities for a larger scattering angle, $\theta = 73.8^\circ$. According to the behaviour in terms of $j_1(qR_N)$, the oscillations in the cross section have a shorter period in k_i (respectively, in E_e) than for the smaller angle. Even in R , faint structures are now visible at this angle. The difference between electron and positron spin asymmetries decreases with energy at the smaller scattering angle, but the diffraction structures veil this behaviour at the larger angle. In this context it was found [56] that the differential cross section approaches the Born limit (where the difference between electron and positron results tends to zero) when $k_i \rightarrow \infty$, provided that the momentum transfer $q \approx k_i\theta$ is kept constant. But also when q is decreased by reducing θ , the distances between lepton and

nucleus, which are relevant for the scattering process, are getting larger. This weakens the action of the nuclear potential, leading to diminishing electron-positron differences.

In order to study the behaviour of the phase shift between the positron and electron diffraction structures we provide in Fig.3a the energy dependence of the differential cross section for the lead nucleus when the scattering angle is varied systematically. For the sake of an easy change of parameters, when progressing to lighter nuclei, we have chosen a Fermi-type nuclear charge density, $\varrho_F(r) = \varrho_0(1 + e^{(r-c)/a})^{-1}$, which is available for the isotope ^{206}Pb [53]. Significant deviations with respect to the Fourier-Bessel-type charge distribution of the ^{208}Pb nucleus appear only above 400 MeV (for $\theta = 44.1^\circ$, where the more accurate charge density provides better agreement with the electron experiment at 450 MeV), but there is no change of the electron-positron phase shift at the higher E_e . An increase or reduction of the parameter c which describes the nuclear extension has no influence on this phase shift either.

On the other hand, as evident from Fig.3a, an increase of the scattering angle from 44.1° to 178° leads to a significant change of the phase shift, in addition to an increase of the number of oscillations in the given energy interval. In particular, electrons and positrons are in phase near $\theta = 140^\circ$ for the lead nucleus.

When the nuclear charge number Z is reduced, the phase shift changes too. In Fig.3b the results for two lighter nuclei with a Fermi-type charge distribution, ^{88}Sr and ^{20}Ne , are shown in addition to those for ^{206}Pb . It is seen that the phase shift is reduced when Z is decreased, i.e. when the nuclear field is weakened. This is even the case when Z is decreased while the nuclear shape is artificially kept fixed. In that latter case the number of oscillations in the given energy interval remains constant.

The change of phase affects also the polarization correlations. For lead, the variation of R with θ follows from Fig.3c at 178° in comparison with the results for 73.8° (Fig.2c). The Z -dependence of S for 73.8° is evident when Fig.2b for ^{208}Pb is set against Fig.3d for ^{20}Ne . For such a light nucleus there is a notable symmetry between the Sherman function of electrons and positrons, with opposite signs except near the location of the minima. Moreover, there is a marked difference in the peak shape. While for the electrons there is a slow rise to maximum, followed by a steep decrease, this is vice versa for the positrons. This feature, although much weaker, exists also for lead.

C. Positron scattering from nuclei with spin

For nuclei with spin $J_i \neq 0$ there occurs also magnetic scattering which results from the current-current interaction between the colliding particles. In addition to the amplitude f_e for potential scattering, the elastic scattering amplitude consists therefore of the magnetic amplitude, which in DWBA reads for positrons [47]

$$A_{fi,e^+}^{\text{mag}}(M_i, M_f) = -\frac{1}{c} \int d\mathbf{r}_N d\mathbf{r} \left(\psi_{i,e^+}^{(-)+}(\mathbf{r}, \zeta_i) \boldsymbol{\alpha} \psi_{f,e^+}^{(+)}(\mathbf{r}, \zeta_f) \right) \frac{\overleftrightarrow{I}}{|\mathbf{r} - \mathbf{r}_N|} \left(\phi_{M_f}^+ \mathbf{J}_N(\mathbf{r}_N) \phi_{M_i} \right), \quad (2.12)$$

where M_i and M_f are, respectively, the initial and final nuclear spin projections, $\boldsymbol{\alpha}$ is a vector of Dirac matrices and \overleftrightarrow{I} is the dyadic unit matrix. \mathbf{J}_N denotes the nuclear current operator, ϕ_M the nuclear functions, \mathbf{r}_N is the nuclear coordinate and \mathbf{r} is the positron coordinate. Eq.(2.12) differs from the respective amplitude for electron scattering [23, 57] not only in the lepton transition matrix element, but also in the negative sign in front of the integral.

The nuclear transition matrix element is multipole expanded [57, 58] in terms of the vector spherical harmonics $\mathbf{Y}_{L\lambda}^M$ as defined in [50],

$$\left(\phi_{M_f}^+ \mathbf{J}_N(\mathbf{r}_N) \phi_{M_i} \right) \equiv j_{fi}(\mathbf{r}_N) = -i \sum_{\lambda LM} (J_i M_i L M | J_f M_f) J_{L\lambda}(r_N) \mathbf{Y}_{L\lambda}^M(\hat{\mathbf{r}}_N), \quad (2.13)$$

where we have used that final and initial nuclear spins are identical, $J_f = J_i$. Also the parity is the same for initial and final nuclear states. The multipolarity of the transition is denoted by L . From parity conservation it follows that for the transitions of unnatural parity, i.e. for the transverse magnetic transitions, the condition $(-1)^{L+1} = 1$ with $\lambda = L$ has to be satisfied. The transverse electric transitions (of natural parity) require $(-1)^L = 1$ and $\lambda = L \pm 1$ [59, 60]. The coefficients $J_{L\lambda}$ are the nuclear ground-state current densities which can either be obtained from the measured cross sections at the backmost scattering angles, or they have to be calculated from nuclear models (see, e.g., [59, 60]).

In the following we will only consider the transverse magnetic transitions, since transverse electric transitions are small for nearly spherical nuclei or for not too high momentum transfer, as compared to the contribution from potential scattering [61]. Thus the sum in (2.13) extends only over odd $L = \lambda$, with $M = M_f - M_i$, where only those M_f are allowed which are compatible with $|M| \leq L$.

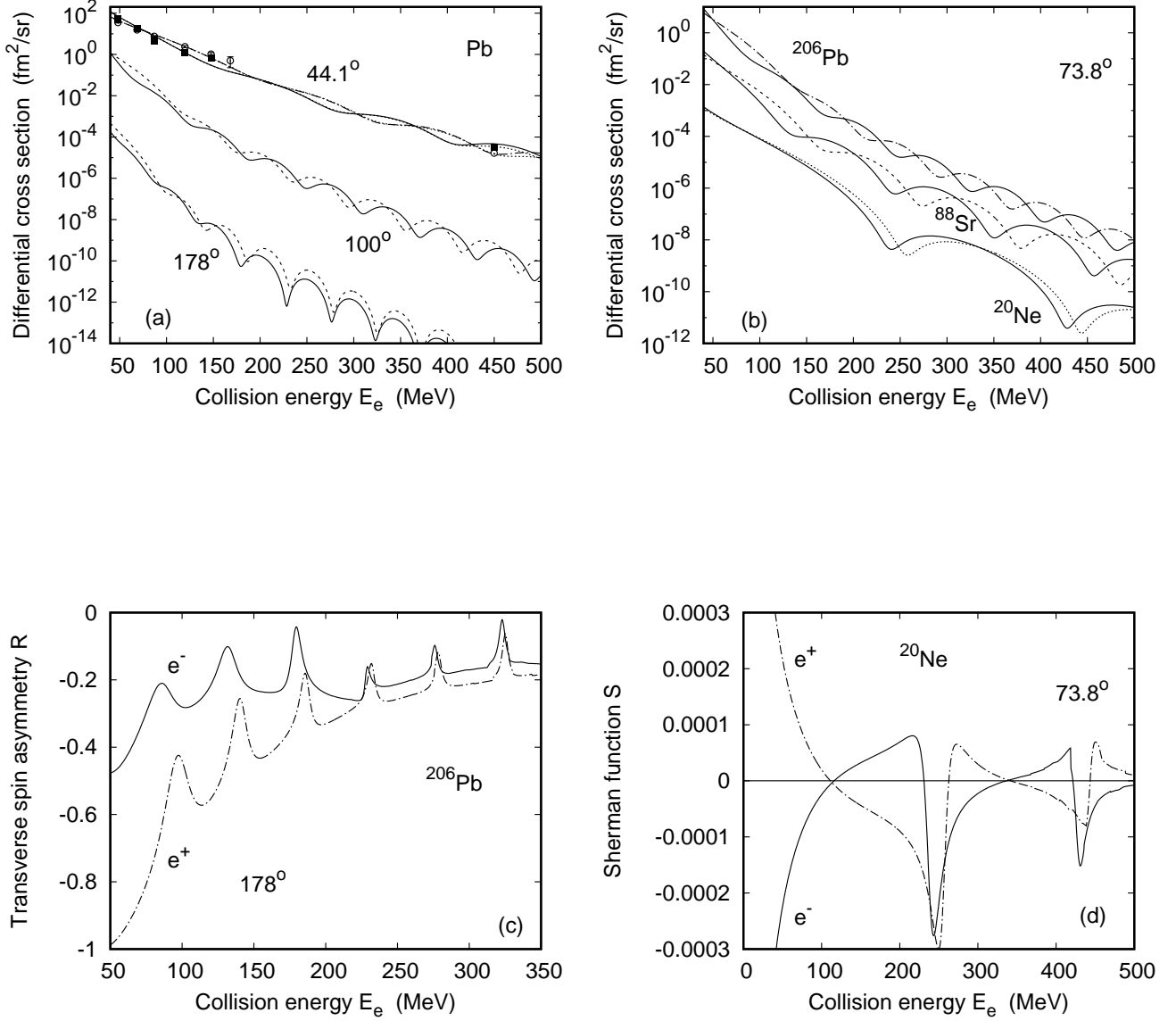


FIG. 3: Differential cross section $\frac{d\sigma}{d\Omega}$ for elastic electron and positron scattering as a function of collision energy E_e for Pb at different scattering angles (a) and at $\theta = 73.8^\circ$ for different targets (b). —, electron results in (a): upper curve, 44.1° ; middle curve, 100° ; lower curve, 178° . Positron results: $-\cdot-\cdot-$, 44.1° ; $-----$, upper curve, 100° ; lower curve, 178° . Experimental data at 44.1° for electrons (■) and positrons (○) are from [8] for $E_e < 200$ MeV, and from [14] at 450 MeV interpolated to $\theta = 44^\circ$. The dotted curves at 44.1° give the results for ^{208}Pb using the Fourier-Bessel type charge density. —, electron results in (b): upper curve, ^{206}Pb ($Z = 82$); middle curve, ^{88}Sr ($Z = 38$); lower curve, ^{20}Ne ($Z = 10$). Positron results: $-\cdot-\cdot-$, ^{206}Pb ; $-----$, ^{88}Sr ; $\cdots\cdots$, ^{20}Ne . For better visibility, the results for Sr are scaled down by a factor of 10, and those for Ne are scaled down by a factor of 100 (e.g. for Ne at 45 MeV, the true cross section is 10^{-1} fm²/sr). (c) shows the spin asymmetry R for ^{206}Pb at $\theta = 178^\circ$ and (d) shows the Sherman function S for ^{20}Ne at $\theta = 73.8^\circ$ as a function of collision energy for electron impact (—) and positron impact ($-\cdot-\cdot-$).

Upon partial-wave expanding the propagator [61],

$$\frac{\overleftrightarrow{I}}{|\mathbf{r} - \mathbf{r}_N|} = \sum_{J\lambda\mu} \frac{4\pi}{2\lambda + 1} \frac{r_{<}^\lambda}{r_{>}^{\lambda+1}} \mathbf{Y}_{J\lambda}^\mu(\hat{\mathbf{r}}) \mathbf{Y}_{J\lambda}^{\mu*}(\hat{\mathbf{r}}_N), \quad (2.14)$$

where $r_< = \min\{r, r_N\}$ and $r_> = \max\{r, r_N\}$, inserting the multipole expansion (2.13) and integrating over the nuclear solid angle, the operator for the positron scattering turns into

$$\begin{aligned} & \int d\Omega_N \boldsymbol{\alpha} \frac{\overleftrightarrow{I}}{|\mathbf{r} - \mathbf{r}_N|} \left(\phi_{M_f}^+ \mathbf{J}_N(\mathbf{r}_N) \phi_{M_i} \right) \\ &= -i \sum_L \frac{4\pi}{2L+1} (J_i M_i L M | J_i M_f) J_{LL}(r_N) \frac{r_<^L}{r_>^{L+1}} \boldsymbol{\alpha} \mathbf{Y}_{LL}^M(\hat{\mathbf{r}}). \end{aligned} \quad (2.15)$$

With the wavefunction representations (2.3) and (2.4) the magnetic amplitude (2.12) for positron scattering is eventually given by

$$\begin{aligned} A_{f_i, e^+}^{\text{mag}}(M_i, M_f) &= -\frac{1}{c} \sum_L \frac{\sqrt{4\pi}}{2L+1} (J_i M_i L M | J_i M_f) \sum_{m_i = \pm \frac{1}{2}} a_{-m_i} (-1)^{\frac{1}{2} - m_i} \\ &\times \sum_{m_s = \pm \frac{1}{2}} b_{-m_s}^* (-1)^{\frac{1}{2} - m_s} \sum_{l_f=0}^{\infty} (-i)^{l_f} Y_{l_f m_l}^*(\hat{\mathbf{k}}_f) \sum_{j_f = l_f \pm \frac{1}{2}} (l_f m_l \frac{1}{2} m_s | j_f m_f) \\ &\times \sum_{\kappa_i} \sqrt{2l_i + 1} i^{l_i} e^{i(\delta_{\kappa_i} + \delta_{\kappa_f})} (l_i 0 \frac{1}{2} m_i | j_i m_i) R_{f_i}(L) W_{12}^{\text{mag}}(l_f, l'_i, L) \end{aligned} \quad (2.16)$$

with the positron angular function

$$\begin{aligned} W_{12}^{\text{mag}}(l_f, l'_i, L) &= \sqrt{\frac{3}{4\pi}} \sqrt{2L+1} (l_f 0 L 0 | l'_i 0) \sqrt{\frac{2l_f+1}{2l'_i+1}} \sum_{m_{s_i} m_{s_f}} (L \mu 1 \varrho | LM) \\ &\times (l'_i \mu_i \frac{1}{2} m_{s_i} | j_i m_i) (l_f \mu_f \frac{1}{2} m_{s_f} | j_f m_f) (\frac{1}{2} m_{s_f} 1 \varrho | \frac{1}{2} m_{s_i}) (l_f \mu_f L \mu | l'_i \mu_i) \end{aligned} \quad (2.17)$$

and the radial integral

$$\begin{aligned} R_{f_i}(L) &= \int_0^{\infty} r_N^2 dr_N J_{LL}(r_N) \int_0^{\infty} r^2 dr \frac{r_<^L}{r_>^{L+1}} [g_{\kappa_f}(r) f_{\kappa_i}(r) + f_{\kappa_f}(r) g_{\kappa_i}(r)] \\ &= \left(\int_0^{\infty} \frac{dr_N}{r_N^{L-1}} J_{LL}(r_N) \int_0^{r_N} dr r^{L+2} + \int_0^{\infty} dr_N r_N^{L+2} J_{LL}(r_N) \int_{r_N}^{\infty} \frac{dr}{r^{L-1}} \right) [g_{\kappa_f}(r) f_{\kappa_i}(r) + f_{\kappa_f}(r) g_{\kappa_i}(r)], \end{aligned} \quad (2.18)$$

where use was made of $W_{12}^{\text{mag}}(l'_f, l_i, L) = -W_{12}^{\text{mag}}(l_f, l'_i, L)$. The sum over L runs from $L = 1$ to $2J_i$ for half-integer J_i in steps of 2. The other variables are determined by the selection rules of the Clebsch-Gordan coefficients,

$$M = M_f - M_i, \quad m_f + M = m_i, \quad m_l = m_f - m_s,$$

$$\mu = \mu_i - \mu_f, \quad \mu_f = m_f - m_{s_f}, \quad \mu_i = m_i - m_{s_i}, \quad \varrho = m_{s_i} - m_{s_f} = M - \mu,$$

$$l_f + L + l'_i = \text{even}. \quad (2.19)$$

For each κ_f , there are $2L+1$ values of κ_i , given by $\kappa_i = (-1)^n \kappa_f + n - (L+1)$ with $n = 1, 2, \dots, 2L+1$.

In fact, the formal shape (2.16) for the positron magnetic amplitude can readily be brought into the formal shape valid for electrons. To do so, one has to revert simultaneously the signs of m_i , m_s , m_{s_i} , m_{s_f} as well as of μ_i , μ_f , m_f , m_l . However, M , ϱ and μ must remain unchanged. Using the symmetry properties of the Clebsch-Gordan coefficients and of the spherical harmonics one ends up with $A_{f_i, e^+}^{\text{mag}}(M_i, M_f)$ differing from the respective

amplitude $A_{fi,e^-}^{\text{mag}}(M_i, M_f)$ for electrons [23] only by a global minus sign, while the Dirac functions f_{κ}, g_{κ} are now eigenfunctions to a potential with sign-reversed nuclear charge number, $-Z$.

The differential cross section for the elastic scattering of polarized positrons into the solid angle $d\Omega$, including recoil in the prefactor and in A_{fi}^{mag} , is obtained from

$$\frac{d\sigma}{d\Omega}(\zeta_i, \zeta_f) = \frac{k_f}{k_i} \frac{1}{f_{\text{rec}}} \frac{1}{2J_i + 1} \sum_{M_i, M_f} \left| A_{fi,e^+}^{\text{coul}} \delta_{M_f, M_i} + \left(4\pi^3 \frac{E_i E_f}{c^2} \right)^{\frac{1}{2}} A_{fi,e^+}^{\text{mag}}(M_i, M_f) \right|^2, \quad (2.20)$$

where A_{fi,e^+}^{coul} , which is only present for $M_f = M_i$, is identified with the elastic scattering amplitude (2.5). Recoil effects are small, implying that the recoil factor f_{rec} [23, 59] is close to unity, and the final total energy E_f differs only slightly from the total energy $E_i = E_e + c^2$ of the impinging particle. When comparing with other literature, it should be noted that the factor $-i$ in the definition (2.13) of the nuclear transition matrix element $j_{fi}(\mathbf{r}_N)$, as well as the replacement of $\mathbf{Y}_{L\lambda}^M$ by $\mathbf{Y}_{L\lambda}^{M*}$ is irrelevant for the cross section.

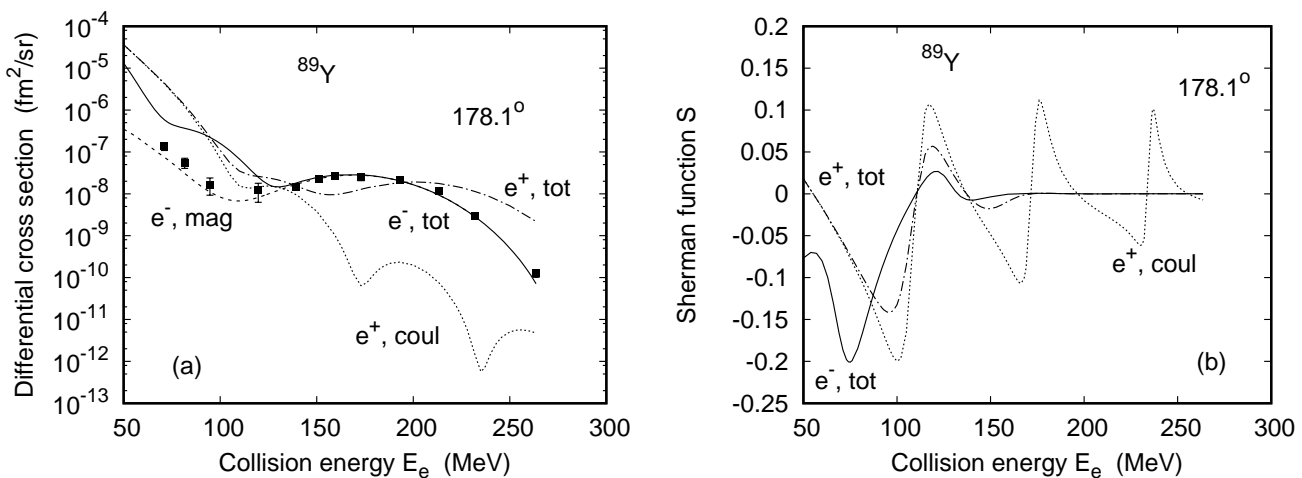


FIG. 4: Differential cross section $\frac{d\sigma}{d\Omega}$ (a) and Sherman function (b) for electrons and positrons scattered elastically from ^{89}Y ($Z = 39$) as a function of collision energy E_e . For theory, the scattering angle is $\theta = 178.1^\circ$. The experimental data in (a) for magnetic electron scattering (which are corrected for the effect of potential scattering) are from Wise et al [43], taken at $\theta = 178.1^\circ$ and 177.6° , respectively. (There is no visible difference in the graph if calculated for 177.6° .) Shown in (a) are for positron scattering the results for the total cross section ($-\cdot-\cdot-$, including Coulombic and magnetic contributions), together with the separate contribution from pure Coulombic scattering ($\cdot\cdot\cdot\cdot$). For electron scattering, $-\cdot-\cdot-$, total cross section; $-\cdot-\cdot-$, magnetic contribution to the cross section.

In (b), the results for S refer to positrons ($-\cdot-\cdot-$, S relating to the total cross section; $\cdot\cdot\cdot\cdot$, S from Coulombic scattering only) and to electrons ($-\cdot-\cdot-$, S relating to the total cross section).

D. Numerical details and results for elastic scattering from ^{89}Y and ^{23}Na

In contrast to potential scattering, the DWBA theory for the magnetic interaction has to meet two difficulties, the convergence of the final-state partial-wave series and the evaluation of the infinite radial integrals. The convergence of these integrals in terms of the upper integration limit is poor for transitions of low multipolarity ($L \lesssim 3$) because of the strongly oscillating integrand. Therefore the complex-plane rotation method (CRM), applied in [39] for nucleon transfer, in [40] for bremsstrahlung and in [62] for nuclear excitation, is used. If in (2.18) the integral from r_N to ∞ is

split at some distance R_m outside the nuclear charge distribution, the second part of this double integral factorizes, isolating the integral

$$\int_{R_m}^{\infty} dr \frac{1}{r^{L-1}} [g_{\kappa_f}(r) f_{\kappa_i}(r) + f_{\kappa_f}(r) g_{\kappa_i}(r)]. \quad (2.21)$$

In the CRM, the real integration path is substituted by a path which follows the positive (or negative) imaginary axis for distances $r > R_m$ and is closed to infinity by the infinitely far semicircle. This is possible because for sufficiently large R_m the solutions f_{κ}, g_{κ} to the Dirac equation can be written as a superposition of regular and irregular Coulomb Dirac functions [54, 55]. These functions can for sufficiently large distances readily be analytically continued into the complex plane where they can be split into a sum of two terms, one vanishing on the infinitely far semicircle of the upper half plane, the other on the respective semicircle in the lower half plane. With the slight inelasticity due to recoil such that $k_i > k_f$, and with $r = R_m \pm iy$, $y > 0$, the resulting complex integrals converge like $\exp(-(k_i - k_f)y)$ [40, 62].

For positron scattering, the partial-wave representation of the Coulomb Dirac functions differs in phase from the one belonging to the attractive potential for electrons. Explicitly, each partial wave, associated with some wave number κ , has to be multiplied by a factor $\delta(\kappa)$ which is given by [54]

$$\delta(\kappa) = \begin{cases} -1, & \kappa < 0 \\ 1, & \kappa > 0 \end{cases} \quad \text{for electrons}$$

$$\delta(\kappa) = 1, \quad \kappa \neq 0 \quad \text{for positrons.} \quad (2.22)$$

This must explicitly be taken care of in the analytical continuation required for the CRM method. In the finite constituents of R_{fi} along real paths, the correct positron phases are automatically accounted for by the numerical solutions of the Dirac equation for negative Z .

For the ^{89}Y nucleus, the nuclear ground-state charge density can again be represented in terms of a Fourier-Bessel expansion [63]. Concerning the magnetic properties, ^{89}Y is characterized by a $2p_{\frac{1}{2}}$ proton outside a closed-shell core and thus has spin $J_i = \frac{1}{2}$. Hence there occurs only a single magnetic ground-state current density, J_{11} . In contrast to earlier work [23] we use here the unscaled J_{11} as provided in [43], since it gives a better fit to the high-energy experimental data for the magnetic electron scattering. When including these experimental results in the figure shown below, their energy positions were extracted from [63], where elastic scattering and nuclear excitation had been measured simultaneously.

Fig.4a displays the differential cross section for electron and positron scattering from ^{89}Y at a scattering angle of 178° as a function of collision energy. For low energies, only the Coulombic (potential) scattering is important. However, already near 100 MeV the magnetic scattering comes into play, and it is dominant above 150 MeV for this angle. The diffraction structures, which are clearly visible in the potential contribution to elastic scattering, are considerably damped in the total cross section. However, the phase shift between the electron and positron results above 100 MeV is very prominent.

In Fig.4b the energy dependence of the Sherman function is shown. While for low collision energies (below 60 MeV) the spin asymmetry for electrons and positrons is of opposite sign, this is no longer true in the regime of the diffraction structures. These oscillations persist also above 150 MeV, but with an amplitude which is strongly damped by the magnetic interaction. Apart from the phase shift between the electron and positron structures, also the shape of the individual peaks is different, which is particularly obvious in the Coulombic contribution to S (see also Figs.2b and 3d).

The angular dependence of the differential cross section and of the polarization correlations S and R is displayed in Fig.5 at a collision energy of 370.9 MeV. At such a high energy the diffraction structures start already at an angle of 30° . Magnetic scattering gains importance at angles near 70° . It also shows diffraction oscillations, however with a much longer period, and at backward angles there is a clear phase shift between the results for electrons and positrons (Fig.5a), as is the case for the total cross section at forward angles (Fig.5b). The influence of magnetic scattering leads to a considerable damping of the diffraction structures above 100° .

Fig.5c compares the angular dependence of the Sherman function for electrons and positrons. There is a significant reduction of $|S|$ above 130° due to the magnetic interaction, particularly for the positrons. This corresponds to the strong increase of the total positron cross section as compared to potential scattering. The diffraction structures are also much less visible for positron impact. This is related to the fact that, due to the repulsive potential, the positron cannot approach the individual protons as much as an electron, weakening the diffraction effects at backward angles.

Finally, the polarization correlation R is displayed in Fig.5d. R is even more sensitive than S to the influence of magnetic scattering, causing a severe reduction of this spin asymmetry already near 100° .

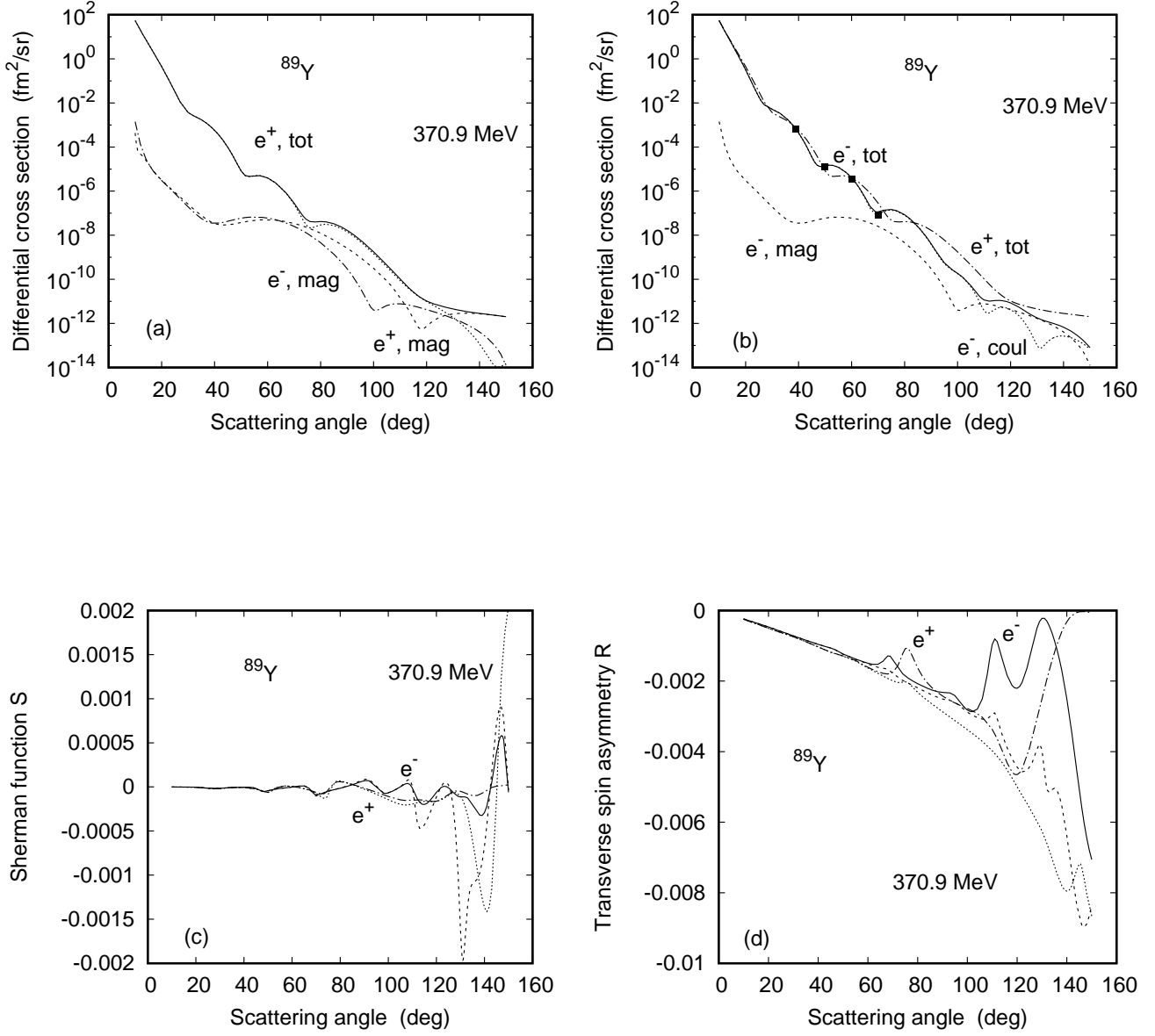


FIG. 5: Differential cross section $\frac{d\sigma}{d\Omega}$ (a) and (b), Sherman function S (c) and spin asymmetry R (d) for 370.9 MeV positrons and electrons scattered elastically from ^{89}Y as a function of scattering angle θ . Shown in (a) are the positron results for the total cross section (—), the Coulombic contribution (·····) and the magnetic contribution (----) to the total cross section. For comparison, the magnetic contribution for electron scattering (---) is shown in addition.

In (b), electron results are shown for the total cross section (—), the Coulombic contribution (·····) and the magnetic contribution (----). The experimental data (■) for the total cross section are from [63]. Included are the results for the total cross section for positron impact (---).

In (c), S for positron scattering refers to spin asymmetries of the total cross section (---) and of the Coulombic contribution (·····). Also shown is S for electron scattering, referring to the total cross section (—) and to the Coulombic contribution (----).

In (d), R is shown for positron scattering (total, ---; Coulombic, ·····) and for electron scattering (total, —; Coulombic, ----).

The nucleus ^{23}Na , chosen as another example of nuclei with large magnetic moments, has a $1d_{\frac{3}{2}}$ odd-proton configuration with a filled $1d_{\frac{5}{2}}$ proton subshell. Its ground-state charge distribution $\varrho(r)$ was obtained from nuclear structure calculations [64] (see also [65, 66]). In contrast to a Fermi-type charge distribution $\varrho_F(r)$ with parameters $c = 2.98$ fm (the charge radius [64]) and $a = 0.49$ fm (such that the rms radius of 2.94 fm is reproduced [53]), $\varrho(r)$ has a pronounced dip at small r .

Since ^{23}Na has spin $J_i = \frac{3}{2}$, the two magnetic current densities J_{11} and J_{33} contribute to the magnetic amplitude. They are obtained from the respective transverse magnetic form factors F_L^T , as provided in [44] and improved in [67], by means of the Fourier-Bessel transform

$$J_{LL}(r) = \frac{2}{\pi} \int_0^\infty q^2 dq F_L^T(q) j_L(qr), \quad (2.23)$$

where j_L is a spherical Bessel function. In order to ensure convergence, a Gaussian tail (decaying with q according to $e^{-b^2 q^2/4}$, where b is the oscillator length) was fitted to the numerically available $F_L^T(q)$ at large q . Likewise, the power law $F_L^T(q) \sim q^L$ for small q was used. For the finite radial integrals in (2.18) an upper cutoff at $r_N = 25$ fm for J_{11} and $r_N = 22$ fm for J_{33} was taken, ensuring that the inverse transformation to (2.23) indeed reproduces $F_L^T(q)$.

Fig.6a displays the energy dependence of the cross section at 70° and 178° , together with the result for potential scattering. While at the forward angle magnetic scattering influences the cross section only in its minimum near 250 MeV, it dominates the cross section at 178° already for energies as low as 60 MeV. Comparing with ^{89}Y at the same angle (Fig.4a) it is seen that for ^{23}Na the magnetic scattering is considerably stronger in the region ranging from 50 MeV to 170 MeV. The phase shift between the positron and the electron results is very similar for 70° and 178° , in contrast to the situation for Pb (Fig.3a) where there exists only potential scattering at all angles.

Included is also the result for electron scattering if the Fermi-type charge density ϱ_F is used instead. While there is hardly any difference for energies below 150 MeV, the minimum near 230 MeV for $\theta = 70^\circ$ is slightly shifted. The deviations increase, however, with energy or with scattering angle, where the inner region of the charge density is probed. The dip in the nuclear-structure charge distribution leads in that region to a considerable decrease of intensity as compared to the results for ϱ_F . For example at 178° , or even more at 150° where potential scattering is not yet suppressed, the Fermi-type results are well below the nuclear structure ones for $E_e > 250$ MeV.

In Figs.6b, 6c and 6d the Sherman function is compared for the two leptons at the three angles 70° , 150° and 178° . For energies below 150 MeV there is a marked symmetry between the electron and positron results for this light nucleus, and at the smallest angle the result is similar to the one for ^{20}Ne (Fig.3d) where only potential scattering takes place. For ^{23}Na the reduction by the magnetic scattering affects just the minimum of S near 240 MeV at that angle. This reduction gets stronger at 150° , and eventually leads to a nearly complete loss of spin asymmetry at the backmost angle, as compared to S from potential scattering, except for a small excursion near 210 MeV. Nevertheless, the Sherman function increases strongly with scattering angle, which is particularly prominent at the lowest energies. However, it is still true in the maximum of $|S|$ around 200-250 MeV. For positrons, this maximum amounts to 2.2×10^{-4} at 70° , 8.2×10^{-4} at 150° and 2.5×10^{-3} at 178° , with similar results for electrons. The influence of different types of nuclear charge distributions is also present in the Sherman function. Against expectation, the changes in S are not more prominent than those in the cross section at energies below 300 MeV. At 150° where the effect is largest, the Fermi-type results are shown in addition (Fig.6c).

3. POSITRON BREMSSTRAHLUNG

Since we use the relativistic partial-wave theory for the calculation of bremsstrahlung, which, in contrast to elastic scattering, involves multiple sums of partial waves, we have to restrict ourselves for reasons of convergence to collision energies below 30 MeV. For such moderate energies it is sufficient to consider only the finite nuclear size, while high-energy effects like magnetic scattering or dynamical recoil for nuclei with spin need not be included. Also kinematical recoil effects are small. As a matter of fact, they are included in the triply differential cross section, while, for the sake of an analytic integration over the positron angles, they are omitted in the doubly differential cross section.

Consideration of the finite nuclear size effects is done by choosing the positron functions, like in the case of elastic scattering, as solutions to the Dirac equation with a potential generated by the nuclear ground-state charge density.

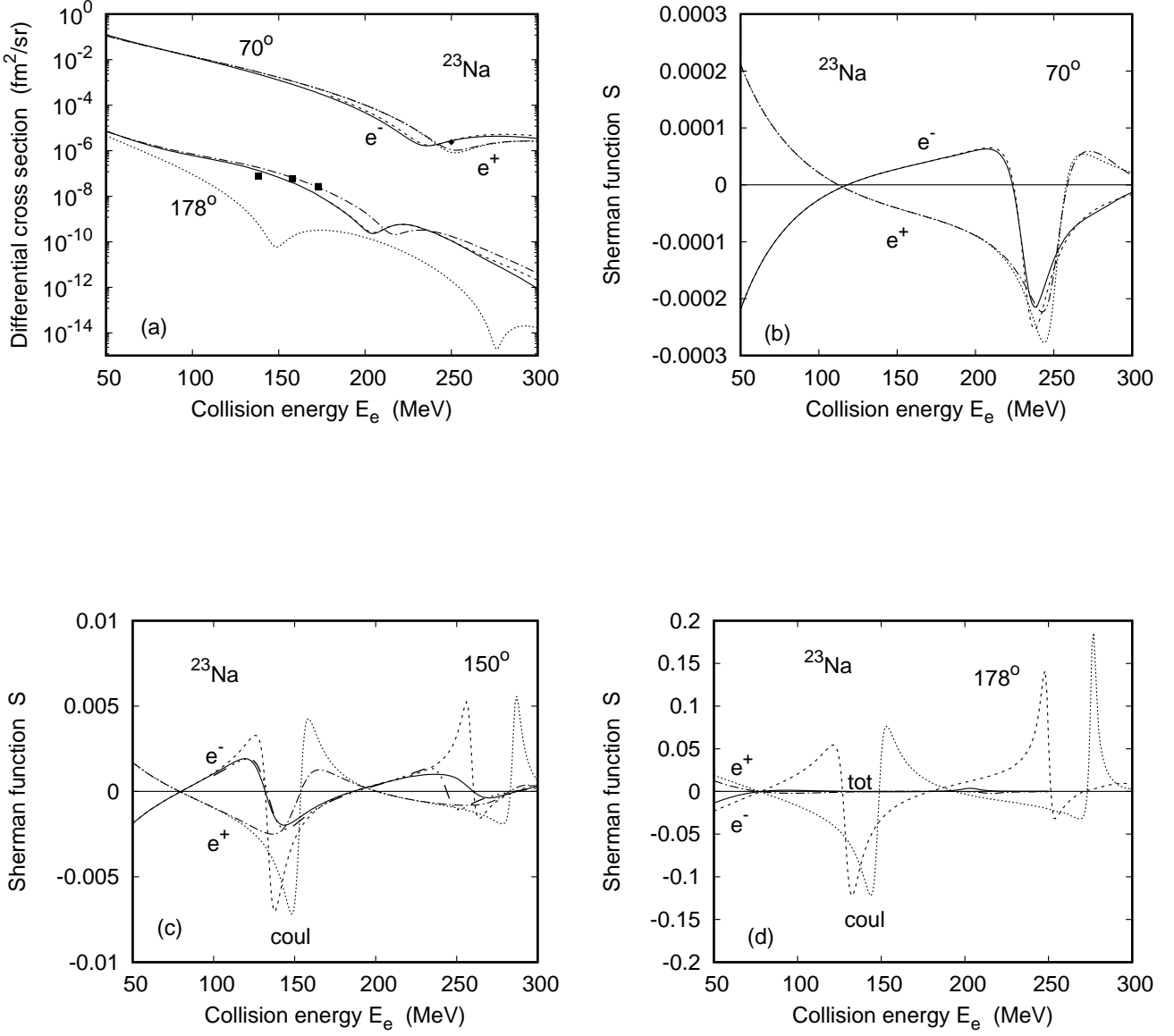


FIG. 6: Differential cross section $\frac{d\sigma}{d\Omega}$ (a) and Sherman function S at scattering angles 70° (b), 150° (c) and 178° (d) for positrons and electrons scattered elastically from ^{23}Na ($Z = 11$) as a function of collision energy E_e . Shown are the results including magnetic scattering for electrons (—) and positrons (- - - -), and the results from positron potential scattering (· · · · ·).

In (a), the upper curves are for 70° and the lower curves for 178° . The total electron cross section results relating to ϱ_F are included (- - - -). The experimental electron data (\blacksquare at 180° , corrected for the effect of potential scattering) are from Torizuka as cited in [44], the datum point (\blacklozenge) at 70° and 250 MeV is interpolated from Singhal et al [44].

In (b), (c) and (d) the spin asymmetry from electron potential scattering (- - - -) is shown in addition. In (c) the results relating to the total electron scattering cross section, but using ϱ_F , are also included (- · · · -).

A. Theoretical description

The radiation matrix element for positron bremsstrahlung is calculated from [32, 47]

$$W_{\text{rad},e^+}(\zeta_i, \zeta_f) = -\frac{ie}{c} \int d\mathbf{r} \psi_{i,e^+}^{(-)+}(\mathbf{r}, \zeta_i) \boldsymbol{\alpha} \boldsymbol{\epsilon}_\lambda^* e^{-i\mathbf{k}\mathbf{r}} \psi_{f,e^+}^{(+)}(\mathbf{r}, \zeta_f), \quad (3.1)$$

with the scattering states $\psi_{i,e^+}^{(-)}$ and $\psi_{f,e^+}^{(+)}$ given in (2.3) and (2.4), respectively. The polarization of the emitted photon is denoted by $\boldsymbol{\epsilon}_\lambda$, and its momentum by \mathbf{k} . When comparing with the magnetic amplitude (2.12) for elastic scattering, it is seen that in both cases the operator $\boldsymbol{\alpha}$ mediates the transition between the initial and final positron spinors. We shall restrict ourselves to the case where the polarization of the scattered positron is not observed and thus has to be summed over. According to the formalism developed for electrons [35, 42], the triply differential cross section for positrons of total energy E_i emitting a photon with frequency $\omega = ck$ into the solid angle $d\Omega_k$, while being scattered with final total energy E_f into the solid angle $d\Omega_f$, is given by

$$\frac{d^3\sigma}{d\omega d\Omega_k d\Omega_f}(\zeta_i, \boldsymbol{\epsilon}_\lambda) = \frac{4\pi^2 \omega k_f E_i E_f}{c^5 k_i f_{\text{re}}} \sum_{m_s = \pm \frac{1}{2}} |F_{f_i, e^+}(\zeta_i, m_s)|^2, \quad (3.2)$$

where f_{re} is a recoil factor close to unity, and F_{f_i, e^+} is defined by means of

$$ic W_{\text{rad},e^+}(\zeta_i, \zeta_f) = \sum_{m_s = \pm \frac{1}{2}} b_{-m_s}^* (-1)^{\frac{1}{2}-m_s} F_{f_i, e^+}(\zeta_i, m_s). \quad (3.3)$$

Upon partial-wave expanding the photon operator [50],

$$e^{-i\mathbf{k}\mathbf{r}} = 4\pi \sum_{l=0}^{\infty} (-i)^l j_l(kr) \sum_{\mu} Y_{l\mu}^*(\hat{\mathbf{k}}) Y_{l\mu}(\hat{\mathbf{r}}), \quad (3.4)$$

where j_l is a spherical Bessel function and $Y_{l\mu}$ a spherical harmonic function, F_{f_i, e^+} turns into

$$\begin{aligned} F_{f_i, e^+}(\zeta_i, m_s) &= \frac{i}{\sqrt{4\pi}} \sum_{l_f=0}^{\infty} \sum_{m_i=-l_f}^{l_f} (-i)^{l_f} Y_{l_f m_i}^*(\hat{\mathbf{k}}_f) \sum_{j_f=l_f \pm \frac{1}{2}} (l_f m_i \frac{1}{2} m_s | j_f m_f) \\ &\times \sum_{m_i = \pm \frac{1}{2}} a_{-m_i} (-1)^{\frac{1}{2}-m_i} \sum_{\kappa_i} \sqrt{2l_i+1} i^{l_i} e^{i(\delta_{\kappa_i} + \delta_{\kappa_f})} (l_i 0 \frac{1}{2} m_i | j_i m_i) S_{f_i, e^+}. \end{aligned} \quad (3.5)$$

In our coordinate system the z -axis is taken along \mathbf{k}_i as before, while the reaction (x, z) -plane is spanned by \mathbf{k}_i and \mathbf{k} , such that $\mathbf{e}_y = \mathbf{k}_i \times \mathbf{k} / |\mathbf{k}_i \times \mathbf{k}|$ and $\mathbf{e}_x = \mathbf{e}_y \times \hat{\mathbf{k}}_i$ with $\hat{\mathbf{k}} = (\sin \theta_k, 0, \cos \theta_k)$ where θ_k is the emission angle of the photon. The final positron momentum \mathbf{k}_f is thus characterized by the spherical angles ϑ_f and φ_f . The factor S_{f_i} includes the sum over the photon angular momenta l ,

$$S_{f_i, e^+} = \sum_{l=|l'_i-l_f|}^{l'_i+l_f} (-i)^l R_{12}(l) W_{12, e^+}(l_f, l'_i, l) - \sum_{l=|l_i-l'_f|}^{l_i+l'_f} (-i)^l R_{21}(l) W_{12, e^+}(l'_f, l_i, l). \quad (3.6)$$

This sum runs in steps of 2 due to the selection rules from the Clebsch-Gordan coefficients in W_{12, e^+} , $l_f + l + l'_i =$ even in the first sum, and $l'_f + l + l_i =$ even in the second one. The radial integrals R_{12} and R_{21} are given by

$$\begin{pmatrix} R_{12}(l) \\ R_{21}(l) \end{pmatrix} = \int_0^\infty r^2 dr j_l(kr) \begin{pmatrix} g_{\kappa_f}(r) f_{\kappa_i}(r) \\ f_{\kappa_f}(r) g_{\kappa_i}(r) \end{pmatrix} \quad (3.7)$$

and agree with the ones for electron scattering (except for the negative charge number in the defining equation of the radial functions), while the functions W_{12, e^+} result from the angular integration,

$$W_{12, e^+}(l_f, l'_i, l) = \sqrt{3} (2l+1) (l_f 0 l 0 | l'_i 0) \sqrt{\frac{2l_f+1}{2l'_i+1}} \sum_{m_s, m_{s_i}} \sqrt{\frac{(l-\mu)!}{(l+\mu)!}} P_l^\mu(\cos \theta_k) c_\rho^{(\lambda)}$$

$$\times (l'_i \mu_i \frac{1}{2} m_{s_i} | j_i m_i) (l_f \mu_f \frac{1}{2} m_{s_f} | j_f m_f) (\frac{1}{2} m_{s_f} 1 \varrho | \frac{1}{2} m_{s_i}) (l_f \mu_f l \mu | l'_i \mu_i), \quad (3.8)$$

where P_l^μ is a Legendre function, using the reduction of $Y_{l\mu}^*(\hat{\mathbf{k}})$ for \mathbf{k} in the reaction plane. The $c_\varrho^{(\lambda)}$ are the coefficients of $\boldsymbol{\epsilon}_\lambda^* = \sum_\varrho c_\varrho^{(\lambda)} \mathbf{e}_\varrho$ in terms of the spherical unit vectors \mathbf{e}_ϱ (with $\varrho = 0, \pm 1$ [50]). For circularly polarized photons, defined by $\boldsymbol{\epsilon}_\lambda \equiv \boldsymbol{\epsilon}^{(\pm)} = \frac{1}{\sqrt{2}} (\boldsymbol{\epsilon}_{\lambda_2} \mp i \boldsymbol{\epsilon}_{\lambda_1})$ with $\boldsymbol{\epsilon}_{\lambda_1} = (0, 1, 0)$ and $\boldsymbol{\epsilon}_{\lambda_2} = (-\cos \theta_k, 0, \sin \theta_k)$ the basis vectors for linear polarization, these coefficients are given by

$$c_\varrho^{(+)} = \begin{cases} \frac{1}{2} (\cos \theta_k - 1), & \varrho = 1 \\ -\frac{1}{2} (\cos \theta_k + 1), & \varrho = -1 \\ \sin \theta_k / \sqrt{2}, & \varrho = 0, \end{cases}$$

$$c_\varrho^{(-)} = \begin{cases} -c_\varrho^{(+)}, & \varrho = \pm 1 \\ c_\varrho^{(+)}, & \varrho = 0 \end{cases}. \quad (3.9)$$

The selection rules for the magnetic quantum numbers imply

$$\mu = \mu_i - \mu_f, \quad \mu_f = m_f - m_{s_f}, \quad \mu_i = m_i - m_{s_i}, \quad \varrho = m_{s_i} - m_{s_f}, \quad m_l = m_f - m_s, \quad (3.10)$$

which is a subset of the relations (2.19).

The interrelation between electron and positron bremsstrahlung turns out to be based on the formal identity,

$$\sum_{m_s} |F_{f_i, e^+}(\boldsymbol{\zeta}_i, m_s)|^2 = \sum_{m_s} |F_{f_i, e^-}(\boldsymbol{\zeta}_i, m_s)|^2, \quad (3.11)$$

taken into consideration that the respective radial integrals as well as the phase shifts differ in the sign of Z .

Eq.(3.11) can be proved by changing in (3.2) simultaneously the sign of all magnetic quantum numbers except for ϱ and μ , and by making use of the symmetry properties of the Clebsch-Gordan coefficients and of the spherical harmonic functions.

For the sake of completeness we provide the explicit result for electron bremsstrahlung, to be inserted into (3.2) in place of F_{f_i, e^+} ,

$$F_{f_i, e^-}(\boldsymbol{\zeta}_i, m_s) = \frac{i}{\sqrt{4\pi}} \sum_{l_f=0}^{\infty} \sum_{m_l=-l_f}^{l_f} (-i)^{l_f} Y_{l_f m_l}(\hat{\mathbf{k}}_f) \sum_{j_f=l_f \pm \frac{1}{2}} (l_f m_l \frac{1}{2} m_s | j_f m_f)$$

$$\times \sum_{m_i=\pm \frac{1}{2}} a_{m_i} \sum_{\kappa_i} \sqrt{2l_i+1} i^{l_i} e^{i(\delta_{\kappa_i} + \delta_{\kappa_f})} (l_i 0 \frac{1}{2} m_i | j_i m_i) S_{f_i, e^-},$$

$$S_{f_i, e^-} = \sum_{l=|l'_i-l_f|}^{l'_i+l_f} (-i)^l R_{12}(l) W_{12, e^-}(l_f, l'_i, l) - \sum_{l=|l_i-l'_f|}^{l_i+l'_f} (-i)^l R_{21}(l) W_{12, e^-}(l'_f, l_i, l), \quad (3.12)$$

where

$$W_{12, e^-}(l_f, l'_i, l) = \sqrt{3} (2l+1) (l'_i 0 l 0 | l_f 0) \sqrt{\frac{2l'_i+1}{2l_f+1}} \sum_{m_{s_f}, m_{s_i}} \sqrt{\frac{(l-\mu)!}{(l+\mu)!}} P_l^\mu(\cos \theta_k) c_\varrho^{(\lambda)}$$

$$\times (l'_i \mu_i \frac{1}{2} m_{s_i} | j_i m_i) (l_f \mu_f \frac{1}{2} m_{s_f} | j_f m_f) (\frac{1}{2} m_{s_i} 1 \varrho | \frac{1}{2} m_{s_f}) (l'_i \mu_i l \mu | l_f \mu_f) \quad (3.13)$$

with

$$\mu = \mu_f - \mu_i, \quad \mu_f = m_f - m_{s_f}, \quad \mu_i = m_i - m_{s_i}, \quad \varrho = m_{s_f} - m_{s_i}, \quad m_l = m_f - m_s. \quad (3.14)$$

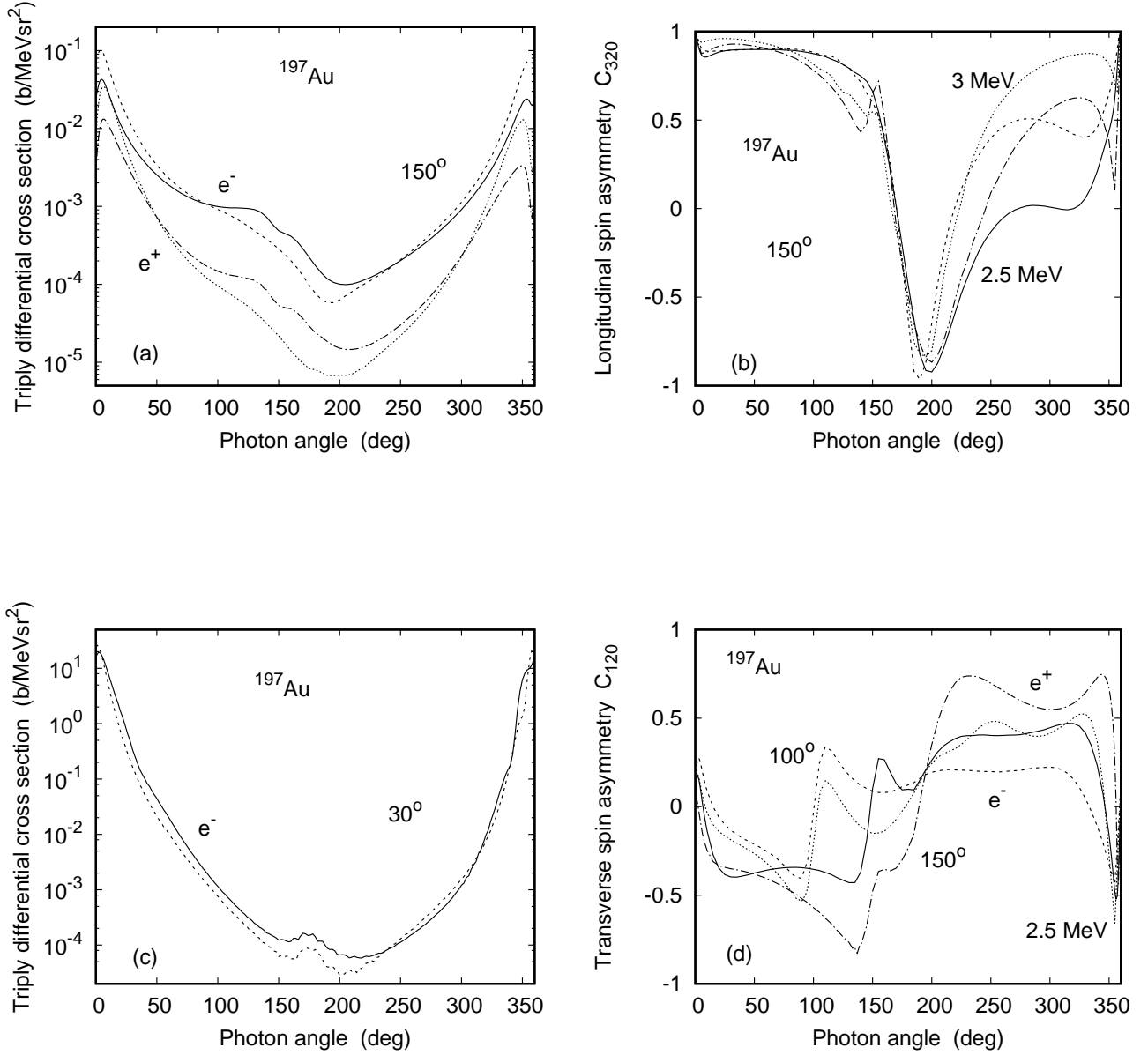


FIG. 7: Triply differential bremsstrahlung cross section $\frac{d^3\sigma}{d\omega d\Omega_k d\Omega_f}$ (a), (c), and polarization correlations C_{320} (b) and C_{120} (d) for 3.5 MeV electrons and positrons colliding with ^{197}Au ($Z = 79$) as a function of photon angle θ_k for coplanar geometry ($\varphi_f = 0$). Shown in (a) and (b) are the results for frequencies $\omega = 2.5$ MeV (—, electrons; - · - · -, positrons) and for $\omega = 3$ MeV (- - - - -, electrons; · · · · ·, positrons) at a scattering angle of $\vartheta_f = 150^\circ$. In (c), the electron cross sections for $\omega = 2.5$ MeV (—) and $\omega = 3$ MeV (- - - - -) are compared at $\vartheta_f = 30^\circ$. Large wiggles near 180° point to numerical uncertainties. In (c) they are partly smoothed by means of averaging over θ_k (over a range $\Delta\theta_k = 10^\circ$). In (d), results are provided for $\omega = 2.5$ MeV and $\vartheta_f = 150^\circ$ (—, electrons; - · - · -, positrons) as well as for $\vartheta_f = 100^\circ$ (- - - - -, electrons; · · · · ·, positrons).

If restriction is made to coplanar emission of photon and positron, such that the azimuthal angle φ_f of the scattered positron (with respect to the reaction plane) is either 0 or 180° , the polarization correlations C_{ij0} between the incoming

positron and the emitted photon are defined in the following way [35],

$$\begin{aligned} \frac{d^3\sigma}{d\omega d\Omega_k d\Omega_f}(\zeta_i, \epsilon_\lambda) &= \frac{1}{2} \left(\frac{d^3\sigma}{d\omega d\Omega_k d\Omega_f} \right)_0 [1 + C_{030}\xi_3 + (C_{110}\xi_1 - C_{120}\xi_2) (\zeta_i e_x) \\ &\quad - (C_{230}\xi_3 + C_{200}) (\zeta_i e_y) - (C_{310}\xi_1 - C_{320}\xi_2) (\zeta_i e_z)], \end{aligned} \quad (3.15)$$

where the prefactor is the cross section for unpolarized particles. The first index in the subscript of C_{ij0} denotes the direction of ζ_i along the coordinate axes e_x , e_y and e_z , while the index 0 refers to unpolarized scattered particles. The second index is associated with the photon polarization, which is defined in terms of the unit vector ξ with coordinates

$$(\xi_1, \xi_2, \xi_3) = (2 \operatorname{Re}(\beta_1 \beta_2^*), 2 \operatorname{Im}(\beta_1 \beta_2^*), |\beta_2|^2 - |\beta_1|^2), \quad (3.16)$$

where β_1 and β_2 are the expansion coefficients of the polarization vector $\epsilon_\lambda = \beta_1 \epsilon_{\lambda_1} + \beta_2 \epsilon_{\lambda_2}$ in terms of the basis vectors ϵ_{λ_1} and ϵ_{λ_2} . When circularly polarized photons are considered, for which $\xi_1 = \xi_3 = 0$, (3.15) reduces to

$$\frac{d^3\sigma}{d\omega d\Omega_k d\Omega_f}(\zeta_i, \epsilon^{(\pm)}) = \frac{1}{2} \left(\frac{d^3\sigma}{d\omega d\Omega_k d\Omega_f} \right)_0 [1 - C_{120}\xi_2 (\zeta_i e_x) - C_{200} (\zeta_i e_y) + C_{320}\xi_2 (\zeta_i e_z)], \quad (3.17)$$

where $\xi_2 = \pm 1$ for $\epsilon^{(\pm)}$.

The polarization correlations C_{ij0} can thus be obtained in terms of relative cross section differences, similar to (2.11), see, e.g. [68].

B. Numerical details and results for bremsstrahlung induced by ^{197}Au and ^{208}Pb

The radial integrals (3.7) are evaluated by applying the CRM like for elastic scattering. Nevertheless, due to the triple sum of partial waves in the transition amplitude the convergence is much poorer, both for collision energies exceeding some tens of MeV, as well as for the emission of soft photons where a large number of final-state partial waves are required. Since for positrons, the electron code can be used with the substitution of $Z \mapsto -Z$ in the nuclear potential and with taking care of the correct partial-wave phases according to (2.22), the description of the numerics given in [42] is valid here too. In some cases, a slightly higher number of partial waves may be required for the positron bremsstrahlung.

In Fig.7 we compare results for 3.5 MeV electron and positron impact on a gold nucleus, for two choices of ω and different scattering angles. Figs.7a and 7b display, respectively, the triply differential cross section and the longitudinal polarization correlation C_{320} for $\vartheta_f = 150^\circ$. Here and in all subsequent figures, the azimuthal angle φ_f of the scattered lepton is set to zero, such that $\theta_k = \vartheta_f$ means parallel emission of photon and lepton. The angles $360^\circ \geq \theta_k > 180^\circ$ are equivalent to setting $\varphi_f = 180^\circ$ for $0 \leq \theta_k < 180^\circ$.

It is seen that for a final kinetic energy $E_f - c^2 = 1$ MeV (corresponding to $\omega = 2.5$ MeV) there is an enhancement of the cross section near $\theta_k = \vartheta_f$, which is reduced to a shoulder at the lower energy ($E_f - c^2 = 0.5$ MeV and $\omega = 3$ MeV).

The positron cross sections are for fixed ω at all photon angles below the ones for electrons due to the repulsive positron-nucleus potential which prohibits too close positron-nucleus encounters and thus reduces the emission of hard photons [31]. Interestingly, for both leptons there is a crossing of the respective bremsstrahlung intensities when changing from $\omega = 2.5$ MeV to 3 MeV at small photon angles ($\theta_k \sim 50^\circ - 80^\circ$, for $\vartheta_f = 150^\circ$) and also at large angles ($250^\circ - 300^\circ$). With decreasing scattering angle, the forward crossing is shifted towards $\theta_k = 0$, while the second crossing moves either closer to 360° (e.g. for $\vartheta_f = 100^\circ$), or it splits into several crossings (e.g. for $\vartheta_f = 30^\circ$, see Fig.7c). This implies that for sufficiently large scattering angles, bremsstrahlung in its region of maximum intensity (close to the beam direction) may have a considerable fraction of photons with high frequency. This is counterintuitive to the general assumption that hard photons are only produced in close lepton-nucleus encounters.

The angular dependence of C_{320} is quite similar for electrons and positrons up to $\theta_k \sim 230^\circ$, except for a pronounced positron peak near 150° (for $\omega = 2.5$ MeV) where the respective cross section has a shallow minimum. However, electron and positron spin asymmetries differ strongly above 270° , even having opposite derivatives with respect to θ_k . The effect of a change in scattering angle at a fixed frequency of 2.5 MeV is displayed in the case of the transverse spin asymmetry C_{120} , see Fig.7d. Clearly, the structure in the photon angular distribution shifts from $\theta_k = 150^\circ$ to 100° when the scattering angle is decreased from $\vartheta_f = 150^\circ$ to 100° . For positrons at $\vartheta_f = 150^\circ$, the peak near $\theta_k = 150^\circ$ is only small, but the maximum spin asymmetry (near 140° , 230° and 340°) is much higher than the one for electrons or the one for positrons at the smaller ϑ_f .

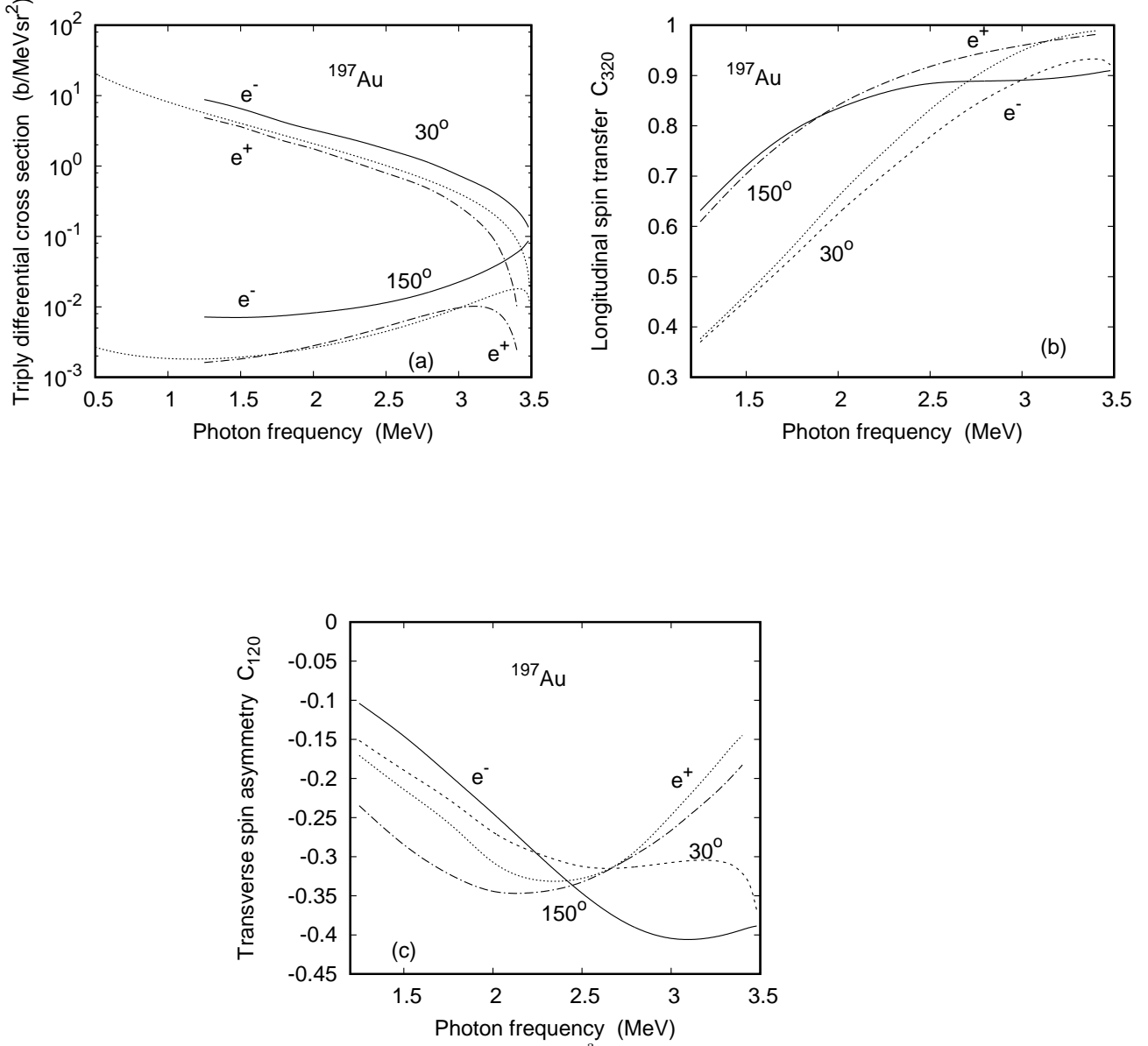


FIG. 8: Triply differential bremsstrahlung cross section $\frac{d^3\sigma}{d\omega d\Omega_k d\Omega_f}$ (a) and polarization correlations C_{320} (b) and C_{120} (c) for 3.5 MeV electrons and positrons colliding with ^{197}Au as a function of photon frequency ω . The photon angle is $\theta_k = 20^\circ$ and $\varphi_f = 0$. In (a) the scattering angle is $\vartheta_f = 30^\circ$ (upper curves) and 150° (lower curves). Shown is the DW for electron impact (—) and for positron impact (---), as well as the PWBA (.....). (b) and (c) provide electron results at 30° (----) and 150° (—) as well as positron results at 30° (.....) and 150° (---).

The frequency dependence of the cross section for the elementary process of bremsstrahlung is shown in Fig.8a at forward photon emission and a forward and backward scattering angle for the same collision system as in Fig.7. At $\vartheta_f = 30^\circ$ the intensity drops monotonously with ω , with its minimum at the SWL. For the positrons, the decrease to zero at the SWL is exponentially, due to the normalization constant of the positron wavefunction [31]. In contrast, at the backward scattering angle the intensity of electron bremsstrahlung *increases* with ω to its maximum at the SWL. For the positron, the intensity peaks near $\omega = 3$ MeV, while the decrease at the higher ω is again due to the normalization constant. This behaviour is in accord with the findings of Fig.6a where for $\vartheta_f = 150^\circ$ at $\theta_k = 20^\circ$ the photons with a higher frequency are preferably emitted.

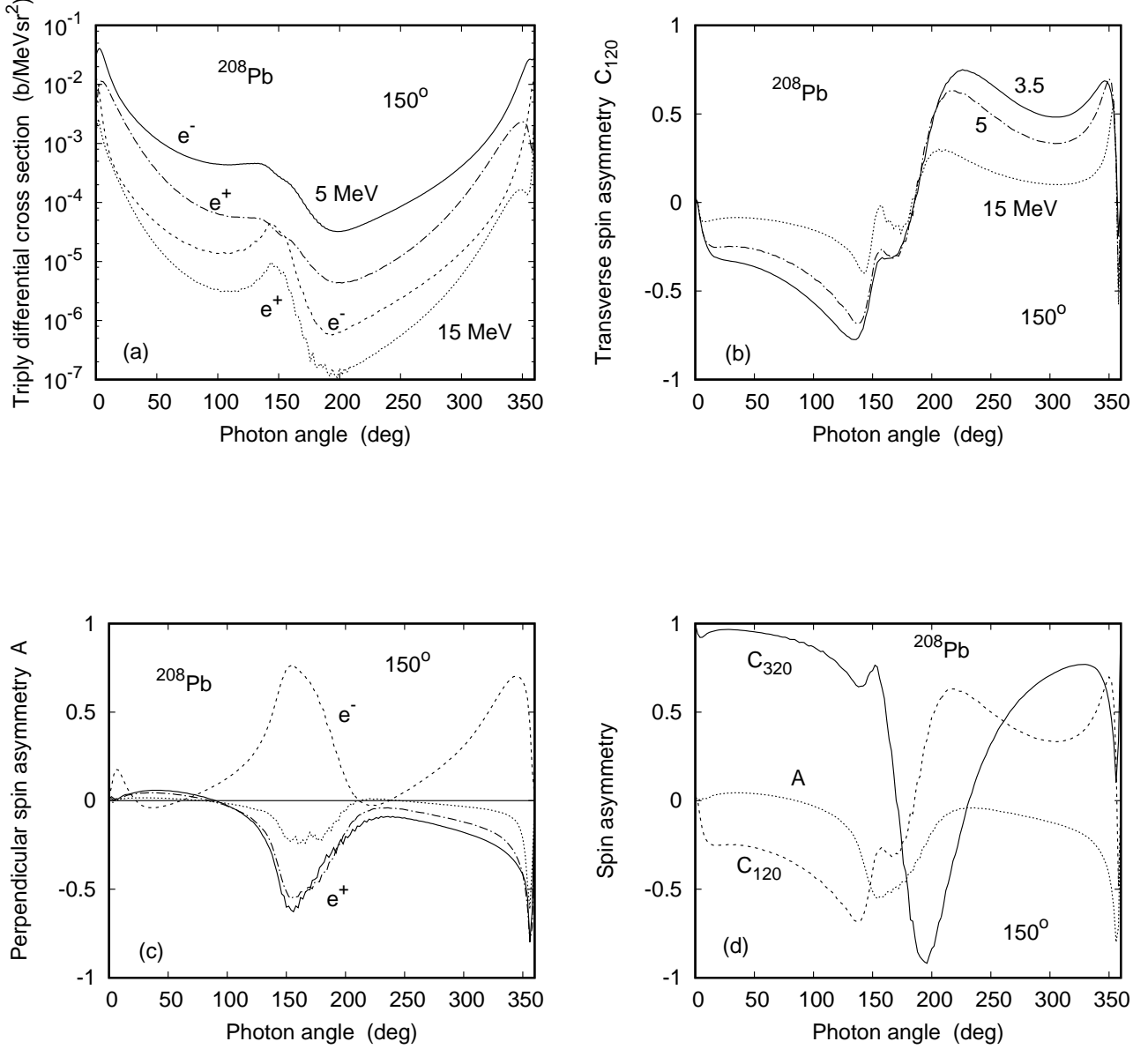


FIG. 9: Triply differential bremsstrahlung cross section $\frac{d^3\sigma}{d\omega d\Omega_k d\Omega_f}$ (a) and polarization correlations C_{120} (b) and $A = C_{200}$ (c) for electrons and positrons colliding with ^{208}Pb at $\vartheta_f = 150^\circ$, $\varphi_f = 0$ as a function of photon angle θ_k . Shown are results for positrons at $E_e = 5$ MeV (---) and 15 MeV (.....). In (a), electron results at 5 MeV (—) and 15 MeV (---) are included. In (b) and (c), positron results at 3.5 MeV (—) are shown in addition. (c) provides also electron results at 3.5 MeV (---).

In (d), the three spin asymmetries C_{320} (—), C_{120} (---) and A (.....) for positrons are shown at $\vartheta_f = 150^\circ$, $\varphi_f = 0$ and $E_e = 5$ MeV. The ratio $\omega/E_e = 3/4$ throughout. The wiggles in C_{120} and A from numerics are partly smoothed by means of averaging over θ_k (over a range $\Delta\theta_k = 10^\circ$).

In order to understand the underlying physics one may study the plane-wave Born approximation (PWBA) for bremsstrahlung where the θ_k -dependence is qualitatively the same as in the DW theory. Since the prefactor of the Bethe-Heitler cross section [49, 69] is proportional to q^{-4} where $\mathbf{q} = \mathbf{k}_i - \mathbf{k}_f - \mathbf{k}$ is the momentum transfer to the nucleus, one expects the cross section to increase with decreasing momentum transfer. In fact, for $\vartheta_f = 150^\circ$, q decreases monotonously with ω (for $\theta_k = 20^\circ$ and $\varphi_f = 0$), corresponding to an increase of the cross section. However,

this increase is considerably weaker than predicted by the inverse power law q^{-4} . Thus the Bethe-Heitler cross section, multiplied by q^4 , is *not* slowly varying with q , but counteracts the q^{-4} -dependence. This fact explains also the decrease of the cross section with ω for $\vartheta_f = 30^\circ$, although at this angle q decreases with ω too, albeit much weaker than for 150° . Hence, hard photons will also be produced at a low momentum transfer, corresponding to a larger lepton-nucleus distance.

The frequency dependence of the polarization correlations C_{320} and C_{120} is shown in Figs.8b and 8c. Like in the case of doubly differential cross sections [37, 70], C_{320} increases monotonously with ω at forward and backward scattering angles. The positron spin asymmetries are higher than those of electrons at $\vartheta_f = 30^\circ$, but lower at 150° if $\omega/E_e \lesssim \frac{1}{2}$. As concerns C_{120} , it decreases monotonously below $\omega = 2$ MeV in all cases, but for high frequencies, $|C_{120}|$ for electrons is much larger at $\vartheta_f = 150^\circ$ than for 30° , while for positrons the increase with ω near the SWL is similar for both angles. If, instead of $\varphi_f = 0$, a coplanar geometry with $\varphi_f = 180^\circ$ is chosen (where lepton and photon emerge on different sides of the beam axis), there appears an interference structure in the photon spectrum for small scattering angles and photon angles (as discussed in [71]), which is also visible in the photon angular distribution near 350° (corresponding to $\theta_k = 10^\circ$ at $\varphi_f = 180^\circ$, see Fig.7c).

In Fig.9 the cross sections and polarization correlations for a ^{208}Pb target are compared at different collision energies for a fixed scattering angle of 150° and for a fixed ratio of ω/E_e . Like for increasing frequency, an increase of collision energy leads to a more pronounced peak in the angular dependent cross section near $\theta_k = \vartheta_f$, whereas the intensity decreases throughout (Fig.9a). It is also seen that the intensity for positron scattering gets closer to the one for electrons when E_e is growing (in concord with the case of unobserved leptons, see Fig.11a below), and the positron structure near 350° is somewhat weakened. Fig.9b shows the variation with E_e of the angular dependent transverse polarization correlation C_{120} for positron impact at the energies 3.5, 5 and 15 MeV, again for the fixed ratio $\omega/E_e = 3/4$. Whereas the global angular variation is reduced with increasing E_e , the peak near 150° is strongly enhanced. The wiggles, particularly in the 15 MeV results, are due to numerical inaccuracies.

In Fig.9c the perpendicular spin asymmetry A is displayed. An increase of the collision energy, as shown for the positrons, leads again to a reduction of the spin asymmetry particularly in the region of its largest excursion near photon angles of 180° and 350° . There is kind of mirror symmetry with respect to the horizontal zero-line between the results for electrons and positrons, shown for $E_e = 3.5$ MeV. The reason lies in the low- Z (or Born) limit where C_{320} and C_{120} are finite (thus implying an identical spin asymmetry for electrons and positrons), while A vanishes in the Born limit and is proportional to Z for low Z . Thus A has mostly opposite signs for electrons and positrons at the moderate collision energies considered for bremsstrahlung. As noted in [32], the symmetry breaking in the polarization correlations between electrons and positrons is due to the strong relativistic effects in high- Z nuclei.

Finally, Fig.9d provides an overview of the three circular polarization correlations for positron impact at $E_e = 5$ MeV as a function of photon angle. Clearly, except for backward angles and near 350° , the longitudinal spin transfer C_{320} is by far the dominating spin asymmetry at such a high collision energy.

C. Polarization sum rule

Based on his work on photoionization, Pratt was able to derive a sum rule for the seven polarization correlations occurring in the doubly differential electron bremsstrahlung, and the numerical verification was provided in [45]. A similar sum rule is valid for the polarization correlations in the triply differential cross section (3.15) [46],

$$C_{320}^2 + C_{120}^2 + C_{200}^2 + C_{030}^2 + C_{310}^2 + C_{110}^2 - C_{230}^2 = 1. \quad (3.18)$$

Since the sum rule is independent of the nuclear potential, it holds also for positrons. While it is strictly verified in the analytic plane-wave Born approximation (PWBA) where all C_{ij0} vanish except for C_{320} , C_{120} and C_{030} [33, 45], numerical inaccuracies occur in the partial-wave theory, particularly for heavy targets and high collision energies, which lead to a violation of (3.18).

As an example we show in Fig.10a the frequency-dependent results for bremsstrahlung at a collision energy of 3.5 MeV. At the forward emission angles, the sum rule is seen to hold numerically within 1% both for electrons and positrons. At larger scattering angles the deviations from unity increase for electrons (but not for positrons) when the frequency falls below 2.5 MeV. From Fig.10b it follows that when also the photon is emitted at large angles, particularly near $\theta_k = 180^\circ$ or 350° , the sum rule is violated by up to 10%. We note that such deviations can be used as a measure of the inaccuracies in the calculations.

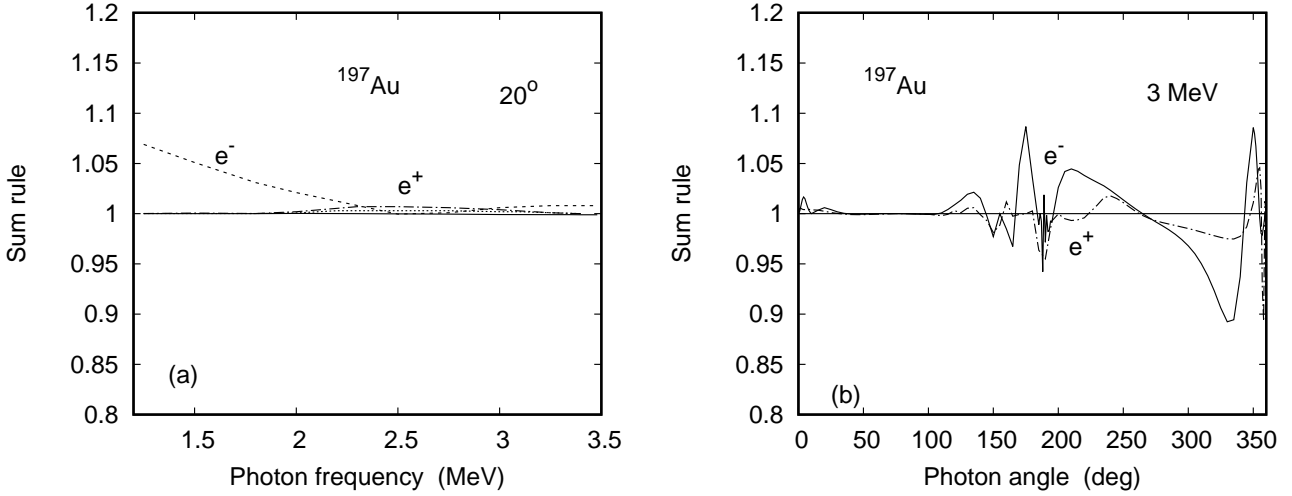


FIG. 10: Lhs of the sum rule (3.18) for bremsstrahlung from 3.5 MeV electrons and positrons colliding with ^{197}Au (a) at $\theta_k = 20^\circ$ as a function of photon frequency ω . The electrons are scattered at 30° (—) and 150° (---), and the positrons at 30° (-·-·-) and 150° (····). In (b), the dependence on photon angle θ_k for $\omega = 3$ MeV and $\vartheta_f = 150^\circ$ is given for electrons (—) and positrons (-·-·-). The azimuthal angle is $\varphi_f = 0$.

D. Doubly differential bremsstrahlung cross section

When only the emitted photon is observed, but not the scattered particle, an integration over the solid angle $d\Omega_f$ has to be performed,

$$\frac{d^2\sigma}{d\omega d\Omega_k}(\zeta_i, \epsilon_\lambda) = \int d\Omega_f \frac{d^3\sigma}{d\omega d\Omega_k d\Omega_f}(\zeta_i, \epsilon_\lambda). \quad (3.19)$$

If recoil is neglected (such that $E_f = E_i - \omega$ is independent of the scattering angle ϑ_f), the partial-wave representation (3.5) of F_{fi} allows for an analytical evaluation of this angular integral, turning the coherent sum over the final-state partial waves into an incoherent one [42].

Fig.11a shows the dependence of the doubly differential cross section on the collision energy for the two photon angles 20° and 140° at a fixed ratio of ω/E_e . It is seen that the cross section decreases monotonously with energy. The positron intensity is again below the electron intensity throughout, and the difference between e^+ and e^- increases with angle and decreases with energy.

Fig.11b displays the polarization correlation C_{32} which tends to 1 at high energies both for electrons and positrons. C_{12} is plotted in Fig.11c. For this polarization correlation the energy dependence of e^+ and e^- is quite different at low collision energies. However, this difference decreases with E_e , being again smaller at the forward angle. Whereas C_{32} and C_{12} have the same sign for electrons and positrons, the perpendicular spin asymmetry A involves a sign change as is seen in Fig.11d. Even more, there is again some symmetry with respect to x -axis for both angles and all energies. The absolute value of the electron-positron difference is also here much smaller for the forward angle than for 140° , while $|A|$ increases with angle. The decrease of the cross section and the increase of $|A|$ with angle points to the increasing importance of close collisions where the relativistic effects are strong. On the other hand, small angles are related to distant collisions, particularly for low photon frequencies. Under such conditions, even the PWBA describes the intensity and the polarization correlations satisfactorily [71]. The maximum value of $|A|$ is below 1 MeV at small angles, while it is near 3 MeV for 140° , its position increasing to about 10 MeV at the backmost angles [68, 72].

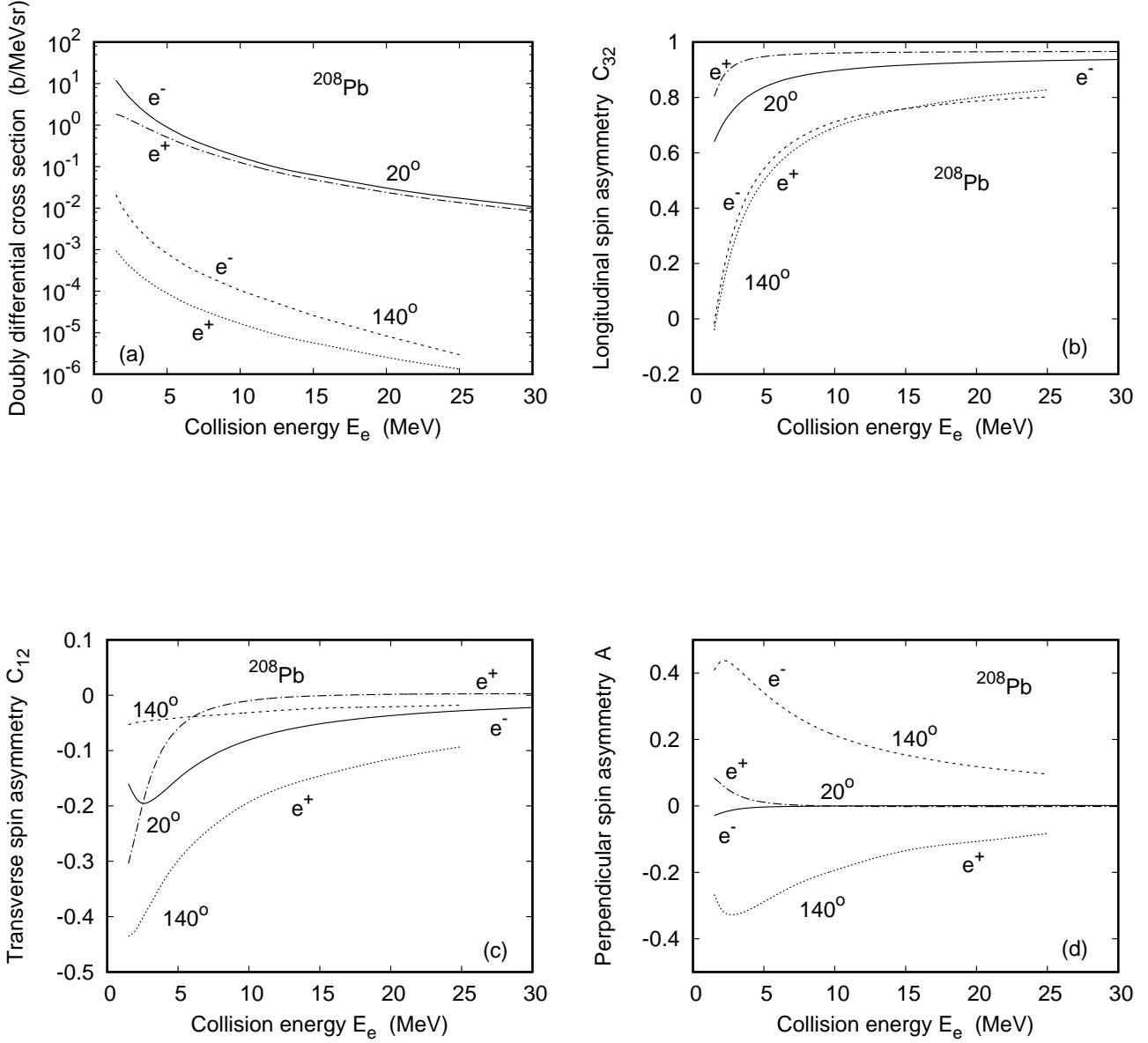


FIG. 11: Doubly differential bremsstrahlung cross section $\frac{d^2\sigma}{d\omega d\Omega_k}$ (a) and polarization correlations C_{32} (b), C_{12} (c) and $A = C_{20}$ (d) for electrons and positrons colliding with ^{208}Pb as a function of collision energy E_e . Shown are results at $\theta_k = 20^\circ$ for electrons (—) and positrons (- - - -) as well as for $\theta_k = 140^\circ$ for electrons (- - - -) and positrons (.....). The ratio $\omega/E_e = 6/7 = 0.857$.

4. CORRESPONDENCE BETWEEN ELASTIC SCATTERING AND BREMSSTRAHLUNG

The photoeffect is a well-known example where the photon acts not as a wave, but as a particle. Bremsstrahlung at the short-wavelength limit (SWL) can be considered as the time-reversed process of photoionization of an electron in a high Rydberg state close to the continuum threshold. Therefore, an SWL photon is also expected to act like a particle. This picture has been confirmed for strong nuclear fields by comparing the polarization correlations of an electron elastically scattered into an angle θ with those of a circularly polarized SWL photon emitted into the same angle, $\theta_k = \theta$. For a gold target and sufficiently high collision energies such that the electron mass can be neglected in the cross section, it turned out that the polarization correlations occurring in elastic scattering (i.e. L, R, S) are

very similar to the ones originating from the doubly differential bremsstrahlung process (C_{32}, C_{12}, A) for identical spin polarization, and their difference decreases with increasing collision energy [28]. Even more, the polarization correlations near the SWL were found to obey an approximate sum rule [28],

$$A^2 + C_{32}^2 + C_{12}^2 \approx 1, \quad (4.1)$$

which corresponds to the strict sum rule for potential scattering [18],

$$S^2 + L^2 + R^2 = 1. \quad (4.2)$$

In order to show that the similarity between the corresponding polarization correlations holds also for positron scattering, we have considered electron and positron scattering from ^{208}Pb at two collision energies, 10 MeV and 15 MeV, and a fixed final energy of 0.1 MeV. Fig.12a provides the angular dependence of the doubly differential bremsstrahlung cross section, showing that close to the SWL the positron cross section is about two orders of magnitude below the electron cross section, due to the suppression of high-energy positron bremsstrahlung by the repulsive positron-nucleus potential.

Fig.12b compares C_{32} and L for 15 MeV electrons and for 10 MeV positrons, and it is seen that for either particle, both C_{32} and L are close to unity up to an angle of 100° , decreasing sharply near 180° . There is also a marked similarity between C_{12} and R (Fig.12c).

Fig.12d shows the respective comparison between A and S (due to a different choice of the coordinate system when originally defining A and S there appears a minus sign in A , such that in fact the shapes of S and $-A$ have to be compared). We have considered electron results for the two collision energies, showing that the minima of both S and $-A$ are located at larger angles and become slightly shallower when E_e is increased. While the positron differences for C_{32} with respect to L and for C_{12} with respect to R are considerably smaller than those for electrons (despite the lower collision energy for positrons which had to be taken due to reasons of convergence), this behaviour is reversed for S with respect to $-A$ even at the same collision energy of 10 MeV. It is also clearly seen that both S and A switch sign when changing from electrons to positrons except at very small angles, while the other polarization correlations do not switch sign. Thus, at high energy, this particular Born-type behaviour remains true for the strong nuclear fields considered here.

5. CONCLUSION

Two basic processes were considered which occur during the scattering of high-energy leptons with heavy nuclei, elastic scattering and bremsstrahlung emission. Both processes were described within the state-of-the-art theories, the relativistic phase shift analysis for elastic scattering supplemented by the DWBA theory to account for magnetic scattering in the case of nuclei with spin, and the relativistic Dirac partial-wave theory for bremsstrahlung.

For elastic scattering, the experimental cross section data for electron and positron impact on lead are well reproduced. We have confirmed the phase shift between electron and positron intensities in the region of the diffraction structures. We have shown that this phase shift increases with potential strength and changes with scattering angle. While the shape of the nuclear charge distribution influences the location of the diffraction minima, it does, however, not alter the electron-positron phase shift.

Comparing the polarization correlations for electrons and positrons, their energy- and angular dependence is much alike in the case of L and R . Existing electron-positron deviations decrease with collision energy but increase with scattering angle. The Sherman function S , on the other hand, differs considerably for the two lepton species. S is not only of opposite sign at low energies and backward scattering angles, but the damping of the diffraction structures in the presence of the magnetic interaction is much stronger for positrons than it is for electrons.

For positron bremsstrahlung no experimental data are yet available, so only predictions could be presented. Due to the repulsive potential, positron bremsstrahlung is much weaker than electron bremsstrahlung, in particular close to the short-wavelength limit. For the triply differential cross section we have found a decrease with frequency ω at forward photon and positron angles as for electron impact or for the doubly differential cross section. However, at backward scattering angles the positron bremsstrahlung intensity increases with ω to a maximum and eventually falls off towards the SWL.

For the circular polarization correlation C_{320} (respectively C_{32} for unobserved leptons) there is a striking similarity between electrons and positrons (like for L in the case of elastic scattering), but for C_{120} there is a large difference between the results for electrons and positrons, particularly at high frequencies where this spin asymmetry is strongly suppressed for the positrons. The behaviour of the spin asymmetry A resembles the Sherman function S for elastic scattering. In particular, it has opposite signs for electrons and positrons in a large parameter region, which lead to

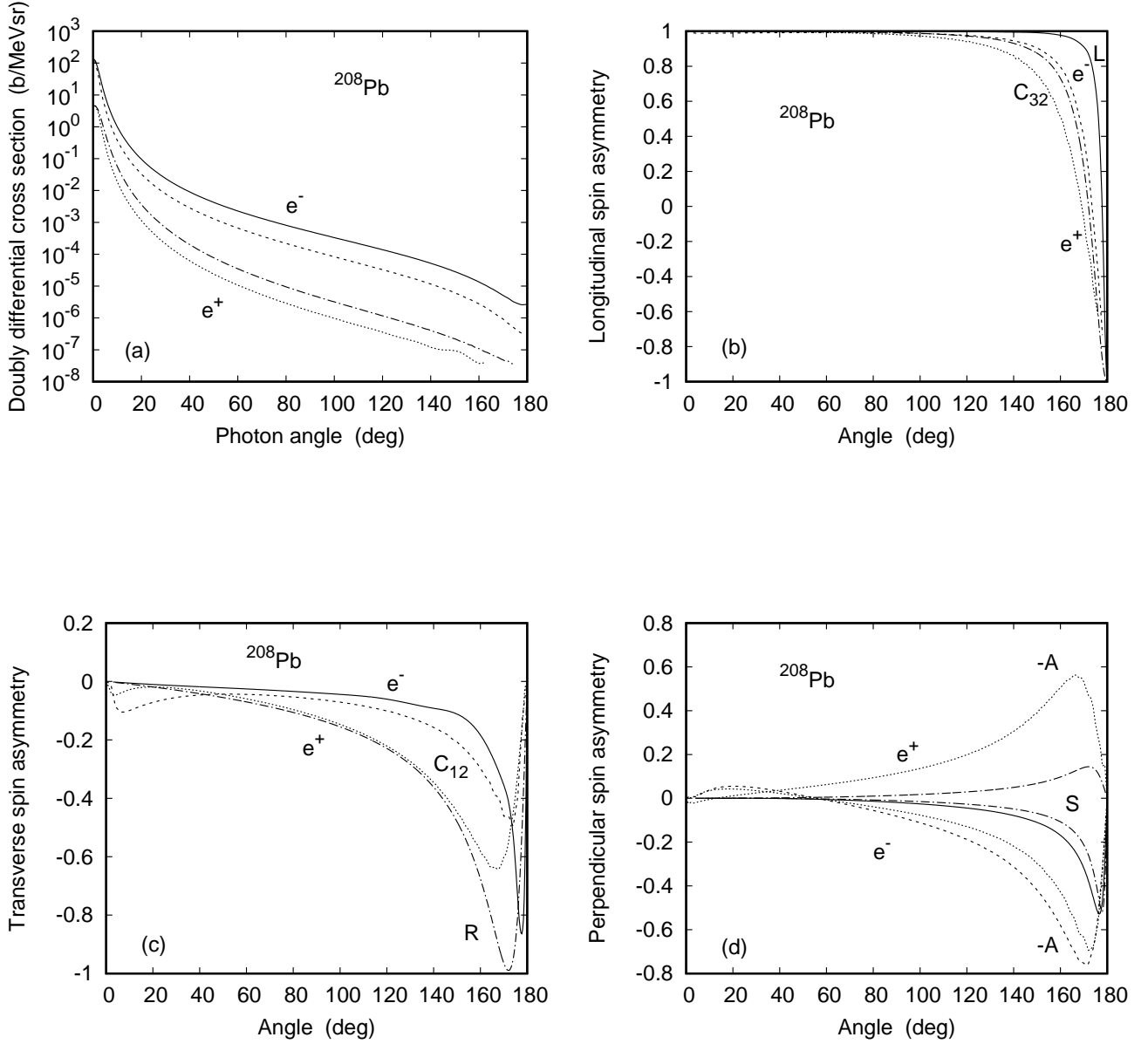


FIG. 12: (a) Doubly differential bremsstrahlung cross section $\frac{d^2\sigma}{d\omega d\Omega_k}$ from electrons and positrons colliding with ^{208}Pb as a function of photon angle θ_k . Shown are results for electron impact at 10 MeV (—) and 15 MeV (---), and for positron impact at 10 MeV (- - - -) and 15 MeV (·····). The final kinetic lepton energy is 0.1 MeV.

(b) Longitudinal spin transfer C_{32} as a function of photon angle θ_k at $E_f - c^2 = 0.1$ MeV and L as a function of scattering angle θ in collision with ^{208}Pb . Shown are results for C_{32} from electrons at 15 MeV (---) and from positrons at 10 MeV (·····), and for L from electrons at 15 MeV (—) and from positrons at 10 MeV (- - - -).

(c) Angular dependence of the transverse polarization correlations C_{12} and R in collision with ^{208}Pb . Shown are results for C_{12} at $E_f - c^2 = 0.1$ MeV from electrons at 15 MeV (---) and from positrons at 10 MeV (·····), and for R from electrons at 15 MeV (—) and from positrons at 10 MeV (- - - -).

(d) Angular dependence of the perpendicular spin asymmetries $A = C_{20}$ and S in collision with ^{208}Pb . Shown are results for $-A$ at $E_f - c^2 = 0.1$ MeV from electrons at 10 MeV (---) and at 15 MeV (·····, lower curve) and from positrons at 10 MeV (·····, upper curve). Results for S are from electrons at 10 MeV (—) and at 15 MeV (- - - -, lower curve) and from positrons at 10 MeV (- - - -, upper curve).

a kind of mirror symmetry with respect to the zero-line in the energy or angular dependence. This behaviour, which is true in the Born approximation valid for low nuclear charge or low frequencies in forward emission, is somewhat unexpected in the case of strong nuclear fields or hard photons.

For electrons, the above-mentioned similarity between the polarization correlations of elastic scattering and the non-coincident bremsstrahlung, for a fixed spin polarization of projectiles and ejectiles, is well-known in case of a complete energy transfer in strong nuclear fields. We have investigated the respective behaviour for positron scattering at a high collision energy E_e and a photon frequency near the SWL, $\omega/E_e = 0.99$. We have found that there is a visible similarity for the pairs L/C_{32} and R/C_{12} , but the differences in the pair S/A are considerably larger for positrons than they are for electrons.

For estimating the precision of the numerical calculations, strict sum rules for the polarization correlations can be applied, both for potential scattering and for the elementary process of bremsstrahlung. While the accuracy is high for elastic scattering (well below one permille for potential scattering, and in the percent region if magnetic scattering is dominant), even at collision energies of 300 MeV or beyond, it is insufficient for bremsstrahlung at backward angles for collision energies as low as 10 – 20 MeV. An accurate bremsstrahlung theory for high-energy projectiles and heavy targets, which goes beyond the PWBA, has still to be awaited.

Acknowledgment

I would like to thank K.Aulenbacher for initiating the positron studies and V.A.Yerokhin for providing additional positron bremsstrahlung results to test my code. I am also indebted to H.Hergert and R.Roth for the nuclear structure calculation of the sodium charge density.

-
- [1] N.J.Mason, J. Phys. D **42**, 194003 (2009)
 - [2] M.J.Kushner, Bull. Am. Phys. Soc. **55**, 107 (2010)
 - [3] K.K.Sharma, Neerja and R.P.Vats, J. At. Mol. Sci. **2**, 294 (2011)
 - [4] K.K.Sharma, Acta Phys. Polonica A **126**, 688 (2014)
 - [5] J.Mar et al, Phys. Rev. Lett. **21**, 482 (1968)
 - [6] J.Arrington, Phys. Rev. C **69**, 032201 (2004)
 - [7] L.R.B.Elton and K.Parker, Proc. Phys. Soc. (London) A **66**, 428 (1953)
 - [8] R.C.Miller and C.S.Robinson, Ann. Phys. N.Y. **2**, 129 (1957)
 - [9] G.H.Rawitscher and C.R.Fischer, Phys. Rev. **122**, 1330 (1961)
 - [10] J.Goldemberg, J.Pine and D.Yount, Phys. Rev. **132**, 406 (1963)
 - [11] R.Hermann, B.C.Clark and D.G.Ravenhall, Phys. Rev. **132**, 414 (1963)
 - [12] A.Baker, Phys. Rev. B **134**, 240 (1964)
 - [13] D.R.Yennie, F.Boos and D.G.Ravenhall, Phys. Rev. B **137**, 882 (1965)
 - [14] V.Breton et al, Phys. Rev. Lett. **66**, 572 (1991)
 - [15] E.-J.Ma et al, Chin. Phys. Lett. **23**, 2695 (2006)
 - [16] H.A.Tolhoek and S.R. de Groot, Physica **17**, 1 (1951)
 - [17] R.Idoeta and F.Legardo, Nucl. Instr. Meth. B **88**, 203 (1994)
 - [18] J.W.Motz, H.Olsen and H.W.Koch, Rev. Mod. Phys. **36**, 881 (1964)
 - [19] H. Überall, *Electron Scattering from Complex Nuclei* (New York: Academic Press) 1971
 - [20] J.Kessler, *Polarized Electrons* (Berlin: Springer) 1976
 - [21] E.D.Cooper and C.J.Horowitz, Phys. Rev. C **72**, 034602 (2005)
 - [22] D.H.Jakubassa-Amundsen and R.Barday, J. Phys. G **39**, 025102 (2012)
 - [23] D.H.Jakubassa-Amundsen, J. Phys. G **41**, 075103 (2014)
 - [24] J.Sromicki et al, Phys. Rev. Lett. **82**, 57 (1999)
 - [25] S.P.Wells et al, Phys. Rev. C **63**, 064001 (2001)
 - [26] L.J.Kaufman, Eur. Phys. J. A **32**, 501 (2007)
 - [27] W.R.Johnson and J.D.Rozics, Phys. Rev. **128**, 192 (1962)
 - [28] D.H.Jakubassa-Amundsen, Phys. Rev. A **85**, 042714 (2012)
 - [29] R.J.Jabbur and R.H.Pratt, Phys. Rev. **129** 184 (1963)
 - [30] R.J.Jabbur and R.H.Pratt, Phys. Rev. **133** B1090 (1964)
 - [31] I.J.Feng, R.H.Pratt and H.K.Tseng, Phys. Rev. A **24** 1358 (1981)
 - [32] V.A.Yerokhin, A.Surzhykov, R.Märtin, S.Tashenov and G.Weber, Phys. Rev. A **86** 032708 (2012)
 - [33] H.K.Tseng and R.H.Pratt, Phys. Rev. A **7** 1502 (1973)
 - [34] C.D.Shaffer, X.-M.Tong and R.H.Pratt, Phys. Rev. A **53** 4158 (1996)
 - [35] H.K.Tseng, J. Phys. B **35** 1129 (2002)
 - [36] O.Kovtun, V.Tioukine, A.Surzhykov, V.A.Yerokhin, B.Cederwall and S.Tashenov, Phys. Rev. A **92**, 062707 (2015)
 - [37] F.Nillius and K.Aulenbacher, Proceedings of Science PSTP2015, 031 (2016)

- [38] H.K.Tseng and R.H.Pratt, Phys. Rev. A **3** 100a(1971)
- [39] C.M.Vincent and H.T.Fortune, Phys. Rev. C **2**, 782 (1070)
- [40] V.A.Yerokhin and A.Surzhykov, Phys. Rev. A **82** 062702 (2010)
- [41] R.A.Müller, V.A.Yerokhin and A.Surzhykov, Phys. Rev. A **90** 032707 (2014)
- [42] D.H.Jakubassa-Amundsen, Phys. Rev. A **93** 052716 (2016)
- [43] J.E.Wise et al, Phys. Rev. C **47**, 2539 (1993)
- [44] R.P.Singhal, A.Watt and R.R.Whitehead, J. Phys. G **8**, 1059 (1982)
- [45] R.H.Pratt, R.A.Müller and A.Surzhykov, Phys. Rev. A **93**, 053421 (2016)
- [46] D.H.Jakubassa-Amundsen, arXiv:1610.09137 [physics.atom-ph] (2016); D.H.Jakubassa-Amundsen, Eur. Phys. J. D **71**: 209 (2017)
- [47] J.D.Bjorken and S.D.Drell, *Relativistic Quantum Mechanics* (New York: McGraw-Hill) 1964
- [48] M.E.Rose, *Relativistic Electron Theory* (New York: Wiley) 1961
- [49] V.B.Berestetskii, E.M.Lifshitz and L.P.Pitaevskii, *Quantum Electrodynamics* Course of Theoretical Physics Vol.4, 2nd edition (Oxford: Elsevier) 1982
- [50] A.R.Edmonds, *Angular Momentum in Quantum Mechanics* 2nd edition (Princeton, NJ: Princeton University Press) 1960
- [51] L.L.Foldy and D.R.Yennie, Phys. Rev. **113**, 1147 (1959)
- [52] N.Sherman, Phys. Rev. **103**, 1601 (1956)
- [53] H.De Vries, C.W.De Jager and C.De Vries, At. Data Nucl. Data Tables **36** 495 (1987)
- [54] F.Salvat, J.M.Fernández-Varea and W.Williamson Jr., Comput. Phys. Commun. **90** 151 (1995)
- [55] D.R.Yennie, D.G.Ravenhall and R.N.Wilson, Phys. Rev. **95**, 500 (1954)
- [56] S.D.Drell and R.H.Pratt, Phys. Rev. **125**, 1394 (1962)
- [57] S.T.Tuan, L.E.Wright and D.S.Onley, Nucl. Instr. Meth. **60**, 70 (1968)
- [58] D.G.Ravenhall and J.Wambach, Nucl. Phys. A **475**, 468 (1987)
- [59] T.W.Donnelly and I.Sick, Rev. Mod. Phys. **56**, 461 (1984)
- [60] J.Heisenberg and H.P.Blok, Ann. Rev. Nucl. Part. Sci. **33**, 569 (1983)
- [61] J.F.Prewitt and L.E.Wright, Phys. Rev. C **9**, 2033 (1974)
- [62] D.H.Jakubassa-Amundsen and V.Yu. Ponomarev, Eur. Phys. J. A **52**: 48 (2016)
- [63] J.E.Wise, F.W.Hersman, J.H.Heisenberg, T.E.Milliman, J.P.Connelly, J.R.Calarco and C.N.Papanicolas, Phys. Rev. C **42**, 1077 (1990)
- [64] R.Roth and H.Hergert, private communication (2017)
- [65] H.Hergert and R.Roth, Phys. Rev. C **80**, 024312 (2009).
- [66] H.Hergert and R.Roth, Phys. Lett. B **682**, 27 (2009).
- [67] K.S.Jassim, A.A.Al-Sammarrae, F.I.Sharrad and H.A.Kassim, Phys. Rev. C **89**, 014304 (2014)
- [68] D.H.Jakubassa-Amundsen, Phys. Rev. A **82**, 042714 (2010)
- [69] H.Bethe and W.Heitler, Proc. Roy. Soc. (London) A **146** 83 (1934)
- [70] D.H.Jakubassa-Amundsen, Phys. Lett. A **375**, 1671 (2011)
- [71] D.H.Jakubassa-Amundsen, J. Phys. B **51**, 055001 (2018)
- [72] D.H.Jakubassa-Amundsen, Phys. Lett. A **377**, 1885 (2013)